NACA

RESEARCH MEMORANDUM

EFFECTS OF HIGH-LIFT DEVICES AND HORIZONTAL-TAIL LOCATION ON

THE LOW-SPEED CHARACTERISTICS OF A LARGE-SCALE 45°

SWEPT-WING AIRPLANE CONFIGURATION

By Ralph L. Maki and Ursel R. Embry

Ames Aeronautical Laboratory
Moffett Field, Calif.

NATIONAL ADVISORY COMMITTEE
FOR AERONAUTICS
WASHINGTON
August 18, 1954

NATIONAL ADVISORY COMMITTEE FOR AERONAUTICS

RESEARCH MEMORANDUM

EFFECTS OF HIGH-LIFT DEVICES AND HORIZONTAL-TAIL LOCATION ON

THE LOW-SPEED CHARACTERISTICS OF A LARGE-SCALE 45°

SWEPT-WING AIRPLANE CONFIGURATION

By Ralph L. Maki and Ursel R. Embry

SUMMARY

A low-speed investigation was made of a large-scale model with a 45° swept wing of aspect ratio 3.5 and taper ratio 0.3. Wing-fuselage configurations with high-lift devices designed to delay the occurrence of stalled flow to a specific high lift coefficient (1.4) at a specific angle of attack (14°) were tested. Tests with several vertical positions of a horizontal tail were made to determine the effects of tail height on the wing-body-tail pitching-moment characteristics after the appearance of stalled flow.

The method outlined in NACA RM A51E15 for estimating the lift coefficient for initial section stall was used to select combinations of high-lift devices capable of providing the required wing lift increments to meet the design criteria. Lift-coefficient values predicted by the method were increased by an empirical factor to account for the consistent conservatism of the method. Double-slotted trailing-edge flaps and leading-edge slats and two section modifications were selected for testing. The measured results gave values of lift coefficient for initial section stall within 0.01 to 0.08 of the predicted values for the high-lift configurations. The basic model (no high-lift devices) showed the largest deviation (0.12).

Tests of the model with the horizontal tail at various vertical locations showed that the lowest height tested (in the wing-chord plane, extended) had the most favorable effects in counteracting the unstable wing-fuselage pitching-moment characteristics at high lifts. Moderately large rolling-moment coefficients (0.02 to 0.03) were measured for the model with cambered wing leading edges and flaps deflected. A half-span wing chord extension tested on one of these configurations successfully reduced the rolling moments.

INTRODUCTION

A major problem in providing satisfactory low-speed aerodynamic characteristics of sweptback wing aircraft is that of overcoming the adverse effects of stalled flow occurring considerably prior to maximum lift. Two general approaches have been used; namely, (1) delay the occurrence of stalled flow to higher lifts, and/or (2) alter the location and rate of progression of the stalled flow. Delays in the occurrence of stalled flow to higher lifts have given the expected result of corresponding delays in the deterioration of the stability, control, and drag characteristics; the variations of the characteristics when stalled flow eventually appears and spreads have generally been found to be unchanged. Alterations in the location and rate of progression of stalled flow have been effective in providing improved longitudinal and lateral-stability characteristics after stall.

The investigation reported herein was concerned with means of delaying stalled flow and means of alleviating the effects of stall on the low-speed aerodynamic characteristics of an airplane model with a 45° sweptback wing of aspect ratio 3.5. A cursory review of current swept-wing airplanes showed that a landing speed of 120 miles per hour, a ground angle of 14°, and a landing wing loading of 50 pounds per square foot were representative values. To approximate these conditions, the design criterion for the model was chosen to be a wing lift coefficient of 1.4 at 14° angle of attack. The primary phase of the investigation was directed toward avoiding any changes in the general character of stability, control, and drag up to this lift coefficient.

A design study is made herein to determine promising wing modifications and high-lift devices. To obtain quantitative estimates of the effectiveness of various wing modifications and high-lift devices in providing delays in the occurrence of stalled flow, use is made of the method of reference 1, modified to a certain extent on the basis of experience in its use. The study indicated that the lift and stall-delay requirements would be satisfied by use of either a full-span airfoil-section modification or a full-span slat, in combination with a partial-span, conventional-type, trailing-edge flap. It had been concluded from preliminary studies that the use of stall-control devices to avoid the probable "pitch-up" changes in wing moment after stall would very likely prevent the attainment of the required lift and the delay in stall. Investigation of means of providing "pitch-down" changes in airplane pitching moment after stall is confined, therefore, to the determination of the effect of vertical location of the horizontal tail.

The report presents the results of tests made to evaluate the effect of airfoil modifications, slats, and trailing-edge flaps (selected on the basis of the design study) on the lift, drag, pitching-moment, and rolling-moment characteristics of the model at zero sideslip. Comparisons are

made of the measured and predicted effectiveness of the modifications and high-lift devices in providing the required lift and delay in stall. The measured effect of vertical location of the horizontal tail is examined and discussed. A brief study of a partial-span chord extension is discussed in connection with the rolling-moment characteristics.

NOTATION

A aspect ratio, $\frac{b^2}{S}$

b span

c wing chord, measured perpendicular to the wing quarter-chord line

c_t tail chord, measured perpendicular to the tail quarter-chord line

c' wing chord, measured parallel to the plane of symmetry

$\bar{c}$ mean aerodynamic chord, $\dfrac{\int_0^{b/2} c'^2 dy}{\int_0^{b/2} c' dy}$

C_D drag coefficient

C_L lift coefficient, referred to basic wing area

C_{La} additional lift coefficient due to angle of attack above 0°

C_{L_1} lift coefficient for initial section stall

C_{Lf} increment of lift coefficient at 0° angle of attack due to flap deflection

$C_{L\alpha}$ lift-curve slope, $\dfrac{dC_L}{d\alpha}$

c_l section lift coefficient

$c_{l_{max}}$ maximum section lift coefficient

C_l rolling-moment coefficient

C_m pitching-moment coefficient referred to a point in the wing-chord plane at the longitudinal station of the wing panel $\bar{c}/4$ points

D   drag

i_t horizontal-tail incidence, measured parallel to the plane of
                symmetry

L   lift

R   Reynolds number, $\dfrac{V\bar{c}}{\nu}$

S   area

V   free-stream velocity

y   spanwise distance from the wing center line

z   distance above the wing-chord plane

α free-stream angle of attack, measured with respect to the
                wing-chord plane

α_1 free-stream angle of attack corresponding to C_{L_1}

ϵ effective angle of downwash, measured with respect to the
                free-stream direction

η spanwise station, $\dfrac{2y}{b}$

ν kinematic viscosity

MODEL AND APPARATUS

Figure 1 is a three-view sketch of the model, showing pertinent
dimensions. Table I is a list of the important geometric data. Table II
gives the surface coordinates of the airfoil section used.

The forward 20-percent and aft 35-percent chord of the wing panels
were removable; the auxiliary leading- and trailing-edge devices were
mounted by removing plain portions and attaching others bearing the
devices. The leading-edge slats and modified sections covered the full
exposed span of the wings. The chord extension was added to one of the
cambered leading edges from 0.5b/2 to the wing tip. Extension of the
slats normal to 0.25c introduced an inboard gap as shown in figure 1.
The trailing-edge flaps extended from 0.159 to 0.693b/2, measured at the
82.5-percent-chord points. Details of the auxiliary devices are shown
in figure 2; the surface coordinates are given in tables III, IV, and V.

The tests were made in the Ames 40- by 80-foot wind tunnel. Figure 3 is a photograph of the model in the test section. Aerodynamic forces were measured with the tunnel six-component balance system.

TESTS AND CORRECTIONS

Lift, drag, pitching-moment, and rolling-moment data were obtained at a free-stream dynamic pressure of 37 lb/sq ft. The Mach number was about 0.16, and the average Reynolds number was 10 million, based on the wing mean aerodynamic chord.

The data have been corrected for stream-angle inclination, wind-tunnel-wall interference, and the approximate interference effects of the support struts. The wall-interference corrections added were as follows:

$$\alpha_T = 0.54 \ C_L$$

$$C_{D_T} = 0.010 \ C_L{}^2$$

$$C_{m_T} = 0.004 \ C_L \ (\text{tail-on data only})$$

DESIGN STUDY

The requirements were that the wing should reach a lift coefficient of 1.4 at 14° angle of attack, without evidencing local section stall. With the specified lift condition a complete airplane with 50 lb/sq ft wing loading would have a landing speed of about 120 mph at a ground angle of 14°.

Calculations were made to determine the types of trailing-edge flaps that might be needed for the wing-fuselage configuration to reach the design lift at the prescribed α, assuming that local section stall would not occur. Having established a suitable trailing-edge flap, estimates were then made to determine leading-edge high-lift devices or airfoil modifications that would provide the required delay in stall.

Selection of Trailing-Edge Flaps

The detailed selection of the trailing-edge flaps was made in the following manner: The lift increment due to angle of attack was calculated using the theoretical wing lift-curve slope given by reference 2 for this wing plan form. This calculation indicated a C_L of only 0.73 would be obtained at $\alpha = 14°$. (For this and succeeding calculations,

the effects of the fuselage were assumed to be minor and were disregarded.) The trailing-edge flaps would thus have to provide an increment of C_L of 0.67 at $\alpha = 14^\circ$. The lift increment, C_{L_f}, given by flaps of various types and area distributions at 0° wing angle of attack were determined by the theory of reference 3. It was considered that the increments would be applicable to the design α of 14° since section stall was to be prevented up to that α. The variation of C_{L_f} with flap span for several types of flaps, each having a chord of 0.25 wing chord and geometrically arranged for best $c_{l_{max}}$, is illustrated in figure 4. It was evident that if flap chords were to be kept to reasonable size, only double-slotted flaps would give the required increment of C_{L_f} of 0.67. (Boundary-layer-control methods were not considered.) The 0.25-chord double-slotted flap represented in figure 4 would serve if the outboard termination were near 0.7 semispan; this flap was selected for testing.

Selection of Leading-Edge Devices

The following procedures were used to select the leading-edge devices and airfoil modifications to provide the required delay in initial section stall: The predictions of the C_L for initial section stall were based on the method of reference 1. In this method, two-dimensional airfoil data are applied by use of simple-sweep-theory concepts and span-load theory. Considerable experience in applying this method has indicated that it consistently underpredicts the lift coefficient for initial section stall on sweptback wings. A study was made of available data for several swept-wing configurations, to obtain a quantitative estimate of the underprediction. The results are summarized in figure 5. The plan forms represented have angles of sweep from 30° to 60°, aspect ratios from 3.4 to 8, and taper ratios from 0.31 to 0.58. From the figure, the following simple percentage corrections were obtained:

$$C_{L_1} \text{ (adjusted)} = K \times C_{L_1} \text{ (unadjusted)}$$

where

K = 1.25 for unflapped wing
K = 1.15 for flapped wing

For the basic model with the double-slotted flaps deflected, C_{L_1} was predicted to be 1.14, and α_1 predicted as 9°. The calculations were based on a two-dimensional $c_{l_{max}}$ of 2.62 for the section with flap, taken from the data in reference 4 without tunnel-wall corrections. The limit c_l distribution outboard of the flaps was drawn by the method suggested in reference 1. The span distribution of c_l at C_{L_1} for this flap span is shown in figure 6 as the solid curve.

Also shown in figure 6 (dashed curves) is the span distribution of c_l required to give a C_{L_1} of 1.40. (Note that the empirical adjustment to the method of reference 1 is made subsequent to drawing the load diagrams, so that for a C_{L_1} of 1.40, the c_l distribution is drawn for a C_L of 1.22.) The peak c_l value on the design lift distribution is 1.57, indicating that a two-dimensional $c_{l_{max}}$ of 3.14 would be required for the section with flap or an additional $c_{l_{max}}$ increment of 0.52 above the $c_{l_{max}}$ of 2.62 reached by the section with a flap.

Of the possible high-lift leading edges, slats and leading-edge modifications were considered. Experimental two-dimensional data were available for the NACA 64A010 section with a slat (ref. 4 and unpublished data). These were used directly to calculate the effect of slat span on C_{L_1}. The results of the computations are shown in figure 7. This plot indicates that if the slats extended from the tip inboard to 0.28 semispan or farther, the wing would exceed the design condition with a C_{L_1} of 1.46.

As no experimental two-dimensional data were available at the time of design for modified leading edges, estimated values of $c_{l_{max}}$ for several modifications were obtained as follows: The peak value of the theoretical pressure distribution (determined by the theory of ref. 5, modified as suggested in ref. 6) for the NACA 64A010 section at its experimental $c_{l_{max}}$ was computed. Theoretical pressure distributions for the section with various increased leading-edge radii and camber were computed for which the peak pressures were equal to that for the unmodified section. The c_l values obtained from these pressure distributions were used as $c_{l_{max}}$ values. Two modified leading-edge designs were chosen with estimated $c_{l_{max}}$ values of 1.62 and 1.71. (See fig. 8.) The increment of $c_{l_{max}}$ provided by the flap on the NACA 64A010 section (1.52) was assumed to be directly additive to the $c_{l_{max}}$ of the sections with modified leading edges. Thus, the flap-deflected $c_{l_{max}}$'s for these sections were estimated as 3.14 and 3.23, respectively. The camber was restricted to the far-forward portion of the chord in one case in the belief that this would offer less chance of adverse high-speed effects. The second modification had more camber than the first, with the camber distributed over a greater portion of the chord. These modifications will be referred to as the 1- and the 2-percent-camber sections, respectively. The predicted values of C_{L_1} for the wing with these modified sections were 1.40 and 1.45 (with flaps deflected), respectively.

RESULTS AND DISCUSSION

Lift and Drag Characteristics

The lift and drag characteristics of the wing-fuselage configurations are presented in figure 9(a) for flaps up and flaps down. The effects of the horizontal tail on the lift and drag are shown in figures 10 to 14.

Of primary interest in the wing-fuselage results are the characteristics of the configurations with high-lift devices compared with the design criterion of C_{L_1} of 1.4 at α_1 of 14°. Predicted and measured values of C_{L_1} and α_1 for these configurations are shown in the following table:

Leading edge	C_{L_1}		α_1, deg	
	Predicted	Measured	Predicted	Measured
Slat	1.46	1.45	15.1	14.8
1-percent camber	1.40	1.32	13.9	11.9
2-percent camber	1.45	1.41	14.9	13.6

The measured values of C_{L_1} were selected as the points at which the drag data indicated the occurrence of section stall. Two of the configurations reached the required lift coefficient and closely approximated the prescribed angle of attack. The third configuration, with the 1-percent-camber sections, fell short of the design condition by an increment of C_L of 0.08, or only 6 percent of the design value. It will be noted that the predicted C_{L_1} values are in each case slightly higher than the measured values. The differences in the α_1 values are somewhat larger, reflecting a small difference between theoretical and measured lift-curve slopes.

A summary of the results for all wing-fuselage configurations tested is shown in table VI. The improvements in the predicted C_{L_1} values when adjusted by the empirical factors are evident in the table. The largest error is for the basic wing configuration. It will be noted that the unflapped configurations tend to be underpredicted and the flapped configurations overpredicted, even though the larger percentage adjustment was applied to the former group. The theoretical value for C_{L_f} of 0.67 agrees with the measured value (fig. 9). In general, these results, together with the correlations shown in figure 5, show that this procedure can be used with considerable confidence for a rapid estimation of C_{L_1} and α_1 for a large range of plan forms.

Pitching-Moment Characteristics and Effective Downwash

Pitching-moment characteristics.- The pitching-moment-coefficient curves for all the configurations with the horizontal tail off had changes in slope in the positive direction beyond C_{L_1}. The expected result was thus obtained that the use of full-span slats and airfoil modifications would not alter the general character of the pitching-moment variations after stall finally begins.

The results of the tests of the model with the horizontal tail on (figs. 10 to 14) show that the low tail position (in the extended wing-chord plane) was best from the standpoint of the pitching-moment variations beyond C_{L_1}. This was true for all model configurations tested. A recent study of a model with a wing of similar plan form, reported in reference 7, indicates that further improvement would be obtained with the horizontal tail somewhat below the wing-chord plane. Comparisons of the lift and pitching-moment characteristics of the various wing configurations with the horizontal tail in the extended wing-chord plane are given in figure 15.

Stabilizer effectiveness and effective downwash.- The effect of varying the tail incidence was investigated on one configuration; the test results are shown in figure 16. The average value of stabilizer effectiveness obtained from these data was assumed to be valid for all configurations throughout the angle-of-attack range and was used to obtain the effective downwash values shown in figure 17. This method of calculation was considered sufficiently accurate to allow a qualitative comparison of the downwash effects. The variation of the downwash with vertical location of the horizontal tail appears to be the reason for the differences in the effect of the horizontal tail. The increase of downwash with α for values of α above α_1 was much greater for the middle and high tail positions, indicating that the lift contributed by the tail was reduced or even reversed as the horizontal tail was raised. Hence, the pitching-moment contributions of the tail became more adverse as the tail was raised.

Rolling-Moment Characteristics

Swept wings tend to stall initially near the wing tips, so any asymmetry in the start or the progression of the stall will develop large rolling moments. The study reported in reference 8 discusses a case where the effects of such rolling moments dominated pilot's opinions of the suitability of the airplane stalling characteristics, overshadowing any effects of the longitudinal instability of the test airplane. The airplane rolling-moment characteristics measured statically in the Ames

40- by 80-foot wind tunnel correlated directly with pilot's opinions of the severity of the stall. It therefore becomes worthwhile to examine the rolling-moment characteristics of the model of this study to determine qualitatively its probable acceptability from the standpoint of roll-off at the stall.

The rolling-moment-coefficient curves for all configurations are given in figures 9 to 14. Those configurations with either of the cambered leading edges with flaps deflected developed maximum C_l values of 0.02 to 0.03 at the start of the stall. Maximum C_l values were generally less than ± 0.01 for the rest of the model configurations. Stall acceptability for the range of C_l values from 0.01 to 0.03 was classified as marginal for the airplane of reference 8. Differences in control effectiveness and airplane rolling moments of inertia from one airplane to another may alter the limits of acceptable rolling-moment coefficient somewhat. However, for an airplane of the type represented by this model, these differences would not be expected to be large enough to alter the acceptable C_l limits materially. It is of interest to note that the larger C_l values occurred with those configurations exhibiting less rounded lift-curve peaks. This agrees with the discussion in reference 8.

The ability of a partial-span, wing, leading-edge, chord extension to improve the rolling-moment characteristics at high lifts is demonstrated in figure 18. It shows that with a half-span chord extension added to the wing with 2-percent-camber sections and flaps deflected, the maximum measured C_l value was reduced from 0.027 to less than 0.01. It will be noted that the drag penalty accruing from use of the extension was negligible. The large gains in C_{L_1} (about 0.05 delay in drag break) and maximum C_L (about 0.1) are deceptive because these coefficients are referred to the area of the basic wing. The rather large chord extension, which increased the wing area by 8 percent, was used to insure the demonstration of C_l improvement without undue testing time.

Performance Characteristics

Some indication of the landing-approach performance characteristics for the model is shown in figure 19 by the lift-drag-ratio curves and the glide sink-speed grid superposed on the drag polars of the configurations with the low horizontal tail. Figure 20 shows the lift characteristics of the model trimmed with a center of gravity located at $0.31\bar{c}$. Values of C_{L_1} are reduced by about 0.12 from the untrimmed values for the flaps-deflected configurations.

CONCLUSIONS

It has been shown that the lift coefficient for the onset of stalled flow on a sweptback wing, with and without high-lift devices, can be predicted by the use of two-dimensional data, simple-sweep concepts, and span-loading theory. Tests showed that a 45° swept-wing model using high-lift devices, with the design based on predictions by this method, met specified lift-coefficient and angle-of-attack requirements within reasonable tolerances.

Unstable wing-fuselage pitching moments were largely controlled by varying the vertical location of the horizontal tail. Of the locations tested, the extended wing-chord plane gave the best results.

Rolling moments at the onset of stall were reduced by the use of partial-span chord extensions.

Ames Aeronautical Laboratory
    National Advisory Committee for Aeronautics
        Moffett Field, Calif., May 10, 1954

REFERENCES

1. Maki, Ralph L.: The Use of Two-Dimensional Section Data to Estimate the Low-Speed Wing Lift Coefficient at Which Section Stall First Appears on a Swept Wing. NACA RM A51E15, 1951.

2. DeYoung, John, and Harper, Charles W.: Theoretical Symmetric Span Loading at Subsonic Speeds for Wings Having Arbitrary Plan Form. NACA Rep. 921, 1948.

3. DeYoung, John: Theoretical Symmetric Span Loading Due to Flap Deflection for Wings of Arbitrary Plan Form at Subsonic Speeds. NACA Rep. 1071, 1952. (Supersedes NACA TN 2278.)

4. Kelly, John A., and Hayter, Nora-Lee F.: Lift and Pitching Moment at Low Speeds of the NACA 64A010 Airfoil Section Equipped with Various Combinations of a Leading-Edge Slat, Leading-Edge Flap, Split Flap, and Double-Slotted Flap. NACA TN 3007, 1953.

5. Allen, H. Julian: General Theory of Airfoil Sections Having Arbitrary Shape or Pressure Distribution. NACA Rep. 833, 1945.

6. Graham, David: A Modification to Thin-Airfoil-Section Theory,
       Applicable to Arbitrary Airfoil Sections, to Account for the
       Effects of Thickness on the Lift Distribution. NACA TN 2298, 1951.

7. Morrison, William D., and Alford, William J., Jr.: Effects of Hori-
       zontal-Tail Height and a Wing Leading-Edge Modification Consisting
       of a Full-Span Nose Flap and a Partial-Span Chord-Extension on the
       Aerodynamic Characteristics in Pitch at High Subsonic Speeds of a
       Model with a 45° Sweptback Wing. NACA RM L53E06, 1953.

8. Anderson, Seth B.: Correlation of Flight and Wind-Tunnel Measure-
       ments of Roll-Off in Low-Speed Stalls on a 35° Swept-Wing Air-
       craft. NACA RM A53G22, 1953.

TABLE I.- GEOMETRIC DATA FOR THE MODEL

Wing

  Area, sq ft. 240.29
  Span, ft 29.00
  Aspect ratio 3.5
  Taper ratio. 0.3
  Mean aerodynamic chord, ft 9.09
  Sweepback of the quarter-chord line, deg 45
  Dihedral angle, deg. 0
  Basic airfoil section, normal to the quarter-
     chord line . . . . NACA 64A010

Trailing-edge double-slotted flap

  Chord in percent of local wing chord, c, constant
     Main flap. 25
     Fore flap. 7.5
  Inboard end of flap, ft from fuselage center line. 2.30
  Outboard end of flap, ft from fuselage center line,
     measured at 82.5-percent chord 10.05

Leading-edge slat

  Chord in percent of local wing chord, c, constant. 17
  Ratio of slat span to wing span. 0.841
  Inboard end of slat, ft from fuselage center line
     Retracted. 2.30
     Extended 3.12

Horizontal tail

  Total area, including blanketed areas, sq ft 72.32
  Span, ft 15.91
  Aspect ratio 3.5
  Taper ratio. 0.3
  Mean aerodynamic chord, ft 4.99
  Sweepback of the quarter-chord line, deg 45
  Sweepback of the axis of rotation, deg 41.77
  Dihedral angle, deg 0
  Airfoil section, normal to the quarter-chord line. . . . NACA 64A010
  Tail length, $\bar{c}/4$ to $\bar{c}_t/4$, ft 13.06
  Volume, $\dfrac{S_t}{S_w} \times \dfrac{\text{tail length}}{\bar{c}}$ 0.43

Fuselage

  Over-all length, ft. 40.48
  Maximum width, ft. 4.46
  Base area, approximate, sq ft. 8.0

TABLE II.- COORDINATES OF THE NACA 64A010 AIRFOIL SECTION

[Dimensions given in percent of airfoil chord,
measured normal to the wing quarter-chord line]

Station	Ordinate
0	0
.5	.804
.75	.969
1.25	1.225
2.5	1.688
5	2.327
7.5	2.805
10	3.199
15	3.813
20	4.272
25	4.606
30	4.837
35	4.968
40	4.995
45	4.894
50	4.684
55	4.388
60	4.021
65	3.597
70	3.127
75	2.623
80	2.103
85	1.582
90	1.062
95	.541
100	.021

L.E. radius: 0.687
T.E. radius: 0.023

NACA

TABLE III.- COORDINATES OF THE WING LEADING-EDGE HIGH-
LIFT DEVICES AND MODIFICATIONS
[Dimensions given in percent of airfoil chord,
measured normal to the wing quarter-chord line]

(a) Slat coordinates

Back of slat		Front of main wing	
Station	Ordinate	Station	Ordinate
4.68	-2.26	4.90	-2.30
5.00	-1.36	5.00	-1.87
5.50	-.56	5.50	-.83
6.00	-.02	6.00	-.24
7.50	1.05	7.50	.91
10.00	2.11	10.00	2.04
15.00	3.46	15.00	3.44
17.00	3.95	17.00	3.95

(b) Surface coordinates for the cambered airfoil sections

Station	Ordinates			
	1-percent camber		2-percent camber	
	Upper	Lower	Upper	Lower
0	-1.12	-1.12	-2.00	-2.00
.25	.36	---	---	---
.50	.65	-1.62	-.58	-2.65
.75	.89	-1.71	-.31	-2.79
1.00	1.09	-1.77	---	---
1.25	1.26	-1.84	.11	-2.99
2.00	1.70	-2.02	---	---
2.50	1.94	-2.15	.91	-3.27
3.50	2.31	-2.40	---	---
5.00	2.72	-2.74	2.02	-3.53
7.50	3.15	-3.15	2.72	-3.62
10.00	3.45	-3.45	3.20	-3.69
15.00	3.94	-3.94	3.90	-3.95
[a]20.00	4.27	-4.27	4.27	-4.27
100.00	.02	-.02	.02	-.02
L.E.radius	1.10		1.10	
Center at	(0.99, -0.64)		(1.06, -1.70)	

[a]Coordinates from 20-percent chord to the
trailing edge are those of the NACA 64A010
section.

TABLE IV.- COORDINATES OF THE WING LEADING-EDGE
CHORD EXTENSION
[Dimensions given in percent of airfoil chord,
measured normal to the wing quarter-chord line]

| Station | Ordinates | |
	Upper	Lower
-15.00	-2.00	-2.00
-14.50	-.55	-2.65
-14.25	-.27	-2.79
-13.75	.14	-2.99
-12.50	.84	-3.19
-10.00	1.63	-3.31
-7.50	2.11	-3.38
-5.00	2.44	-3.44
0	2.94	-3.53
5.00	3.32	-3.60
10.00	3.65	-3.69
15.00	3.96	-3.95
20.00	4.27	-4.27
L.E. radius: 1.10		
Center at (-13.94, -1.70)		

[a]Coordinates from 20-percent
chord to the trailing edge
are those of the NACA 64A010
section.

TABLE V.- COORDINATES OF THE DOUBLE-SLOTTED FLAPS

[Dimensions given in percent of airfoil chord, measured
normal to the wing quarter-chord line]

Main flap			Fore flap		
Station	Ordinates		Station	Ordinates	
	Upper	Lower		Upper	Lower
75.00	-1.00		68.80	0	
75.15	-.37	-1.56	69.22	.95	-0.93
75.30	-.08	-1.71	69.63	1.31	-1.14
75.59	.27	-1.96	70.05	1.52	-1.20
75.88	.54	-2.10	70.47	1.67	-1.11
76.18	.75	-2.18	70.88	1.72	--.85
76.77	1.06	-2.29	71.72	1.74	-.36
77.35	1.27	-2.30	72.55	1.64	-.02
77.94	1.41	-2.30	73.38	1.43	.18
78.53	1.50	-2.26	74.22	1.13	.27
79.71	1.59	-2.14	75.05	.75	.25
80.88	1.64	-2.00	75.88	.28	.11
82.06	1.65	-1.88	76.30	0	0
83.24	1.63	-1.76			
84.41	1.58	-1.64			
85.00	1.55	-1.58	L.E. radius: 1.20		
86.25	1.45	-1.45			
90.00	1.06	-1.06			
95.00	.54	-.54			
100.00	.02	-.02			
L.E. radius: 0.95					
T.E. radius: 0.02					

TABLE VI.- COMPARISONS OF PREDICTED AND MEASURED
VALUES OF C_{L_1} AND α_1

Wing leading edge	$c_{l_{max}}$	C_{L_1}			α_1, deg	
		Predicted		Measured	Predicted	Measured
		Unadjusted	Adjusted			
Without trailing-edge flaps						
Plain	1.10	0.46	0.58	0.70	11.1	12.2
1-percent camber	1.62	.67	.84	.84	16.0	14.6
2-percent camber	1.71	.72	.90	.99	17.2	17.7
Trailing-edge flaps deflected						
Slat	3.26	1.27	1.46	1.45	15.1	14.8
1-percent camber	3.14	1.22	1.40	1.32	13.9	11.9
2-percent camber	3.23	1.26	1.45	1.41	14.9	13.6

Dimensions in feet
except as noted

Double-slotted
flap deflected

45°

Slat
extended

41.8°

2.75

Moment
center

3.26

5.95

45°

$\bar{c}$

$.25\bar{c}_t$

$\bar{c}_t$

.25$\bar{c}$

.25c_t

.25c

90°

Axis of
rotation

NACA 64A010

42.67

23.16

13.06

Moment
center

1.67

3.33

40.48

29.00

15.91

4.46
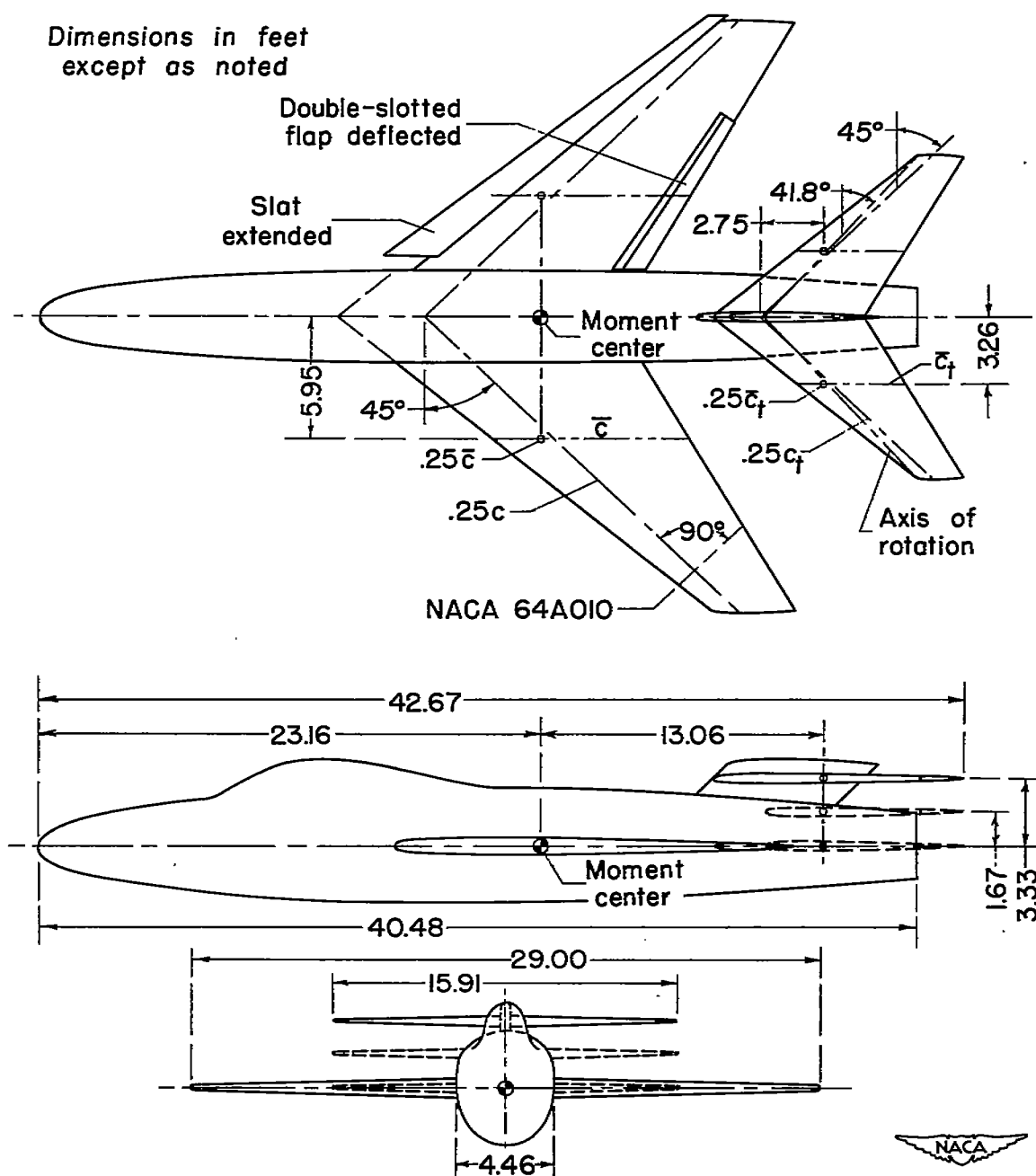
Figure 1.- Three-view sketch of the model.

Slat

.09c   .17c
.015c
.06c
.049c   15°

1-percent-camber section
.0112c
.075c

2-percent-camber section
.020c
.15c

2-percent-camber section with chord extension
.020c
.15c

Sections A-A

.65c
90°
.50 b/2
.25c
90°

Double-slotted flap
.836c
.828c   .010c
.775c   30°   .008c   55°
.863c

Section B-B
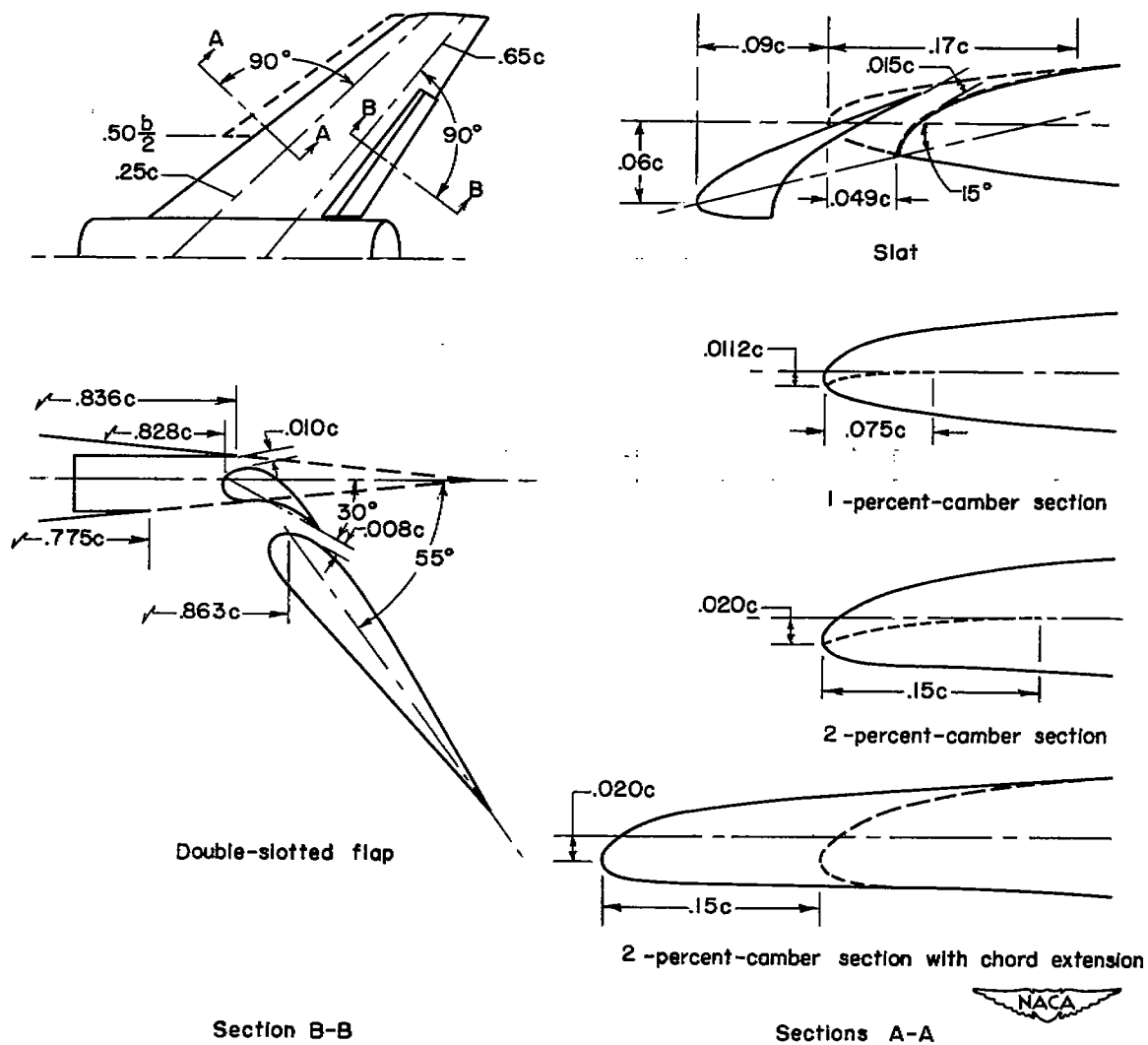
Figure 2.- Details of the various wing leading-edge devices and of the double-slotted wing trailing-edge flaps.
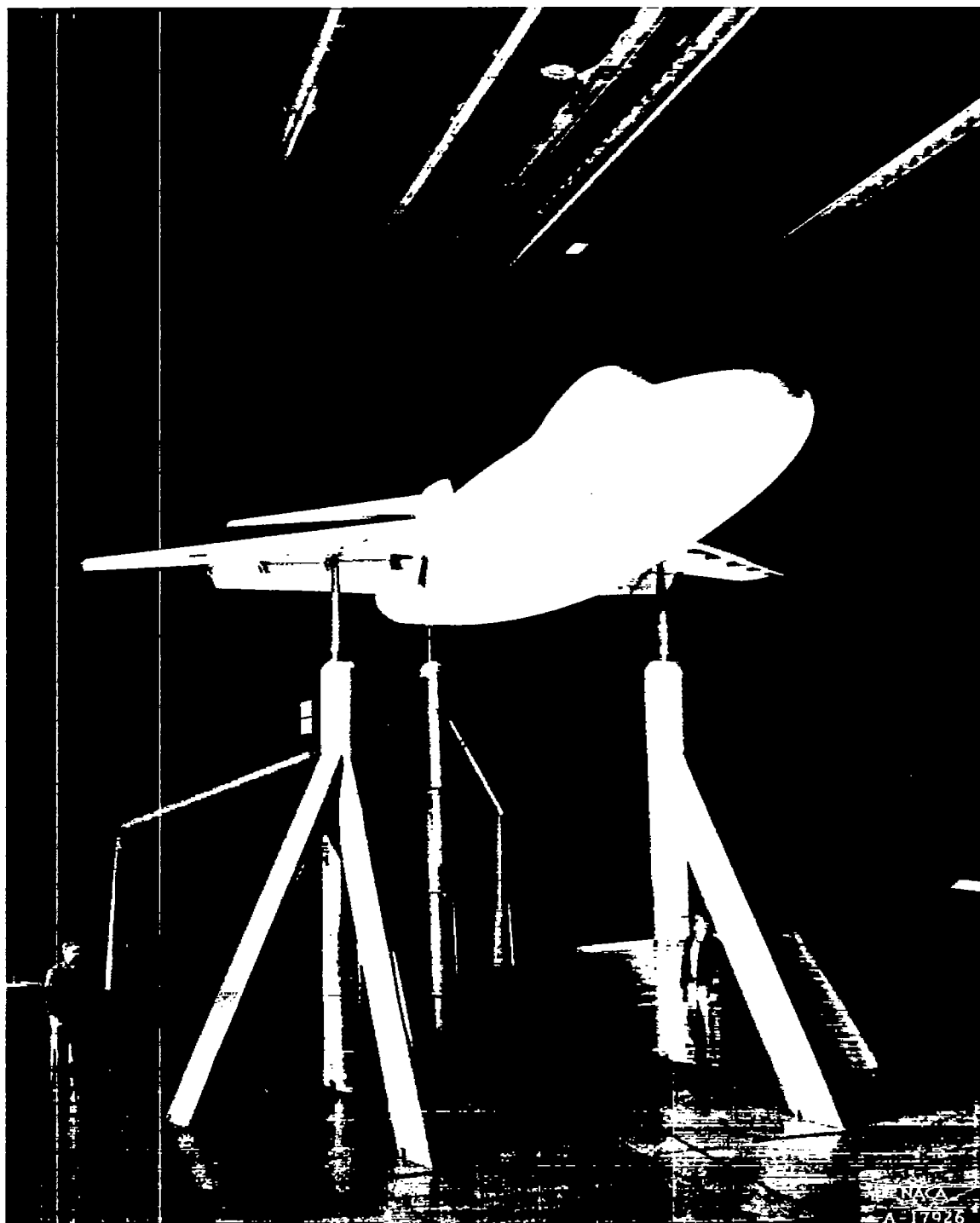
Figure 3.- The model installed in the wind tunnel.
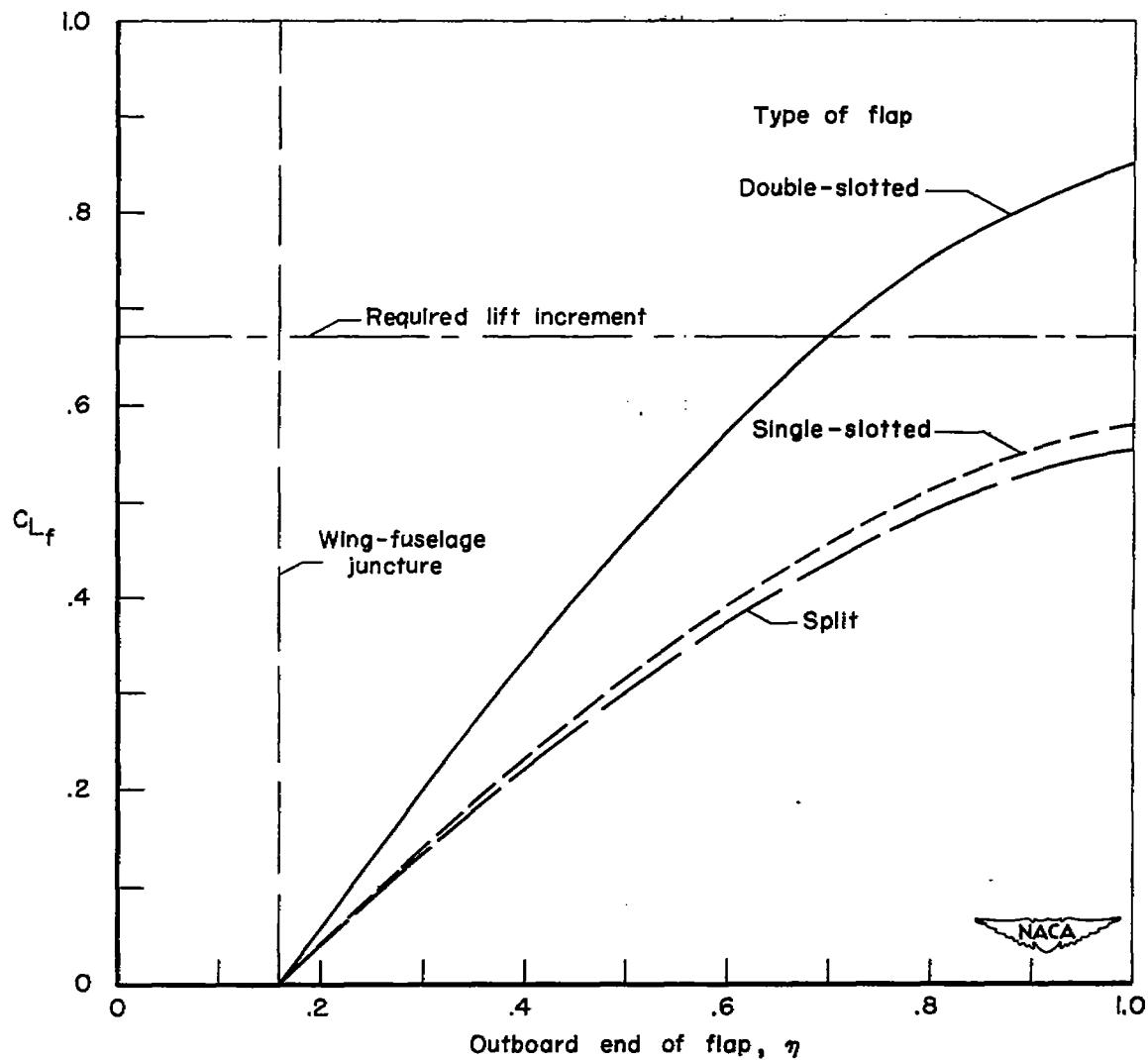
Figure 4.- Variation of flap lift increment at 0° angle of attack with flap span for several types of flaps. Flap-chord ratio of 0.25.
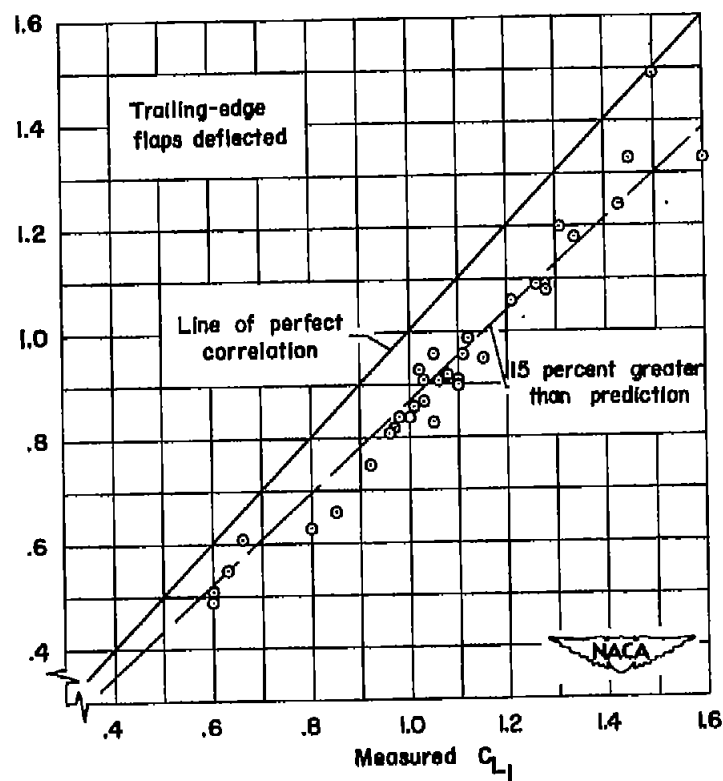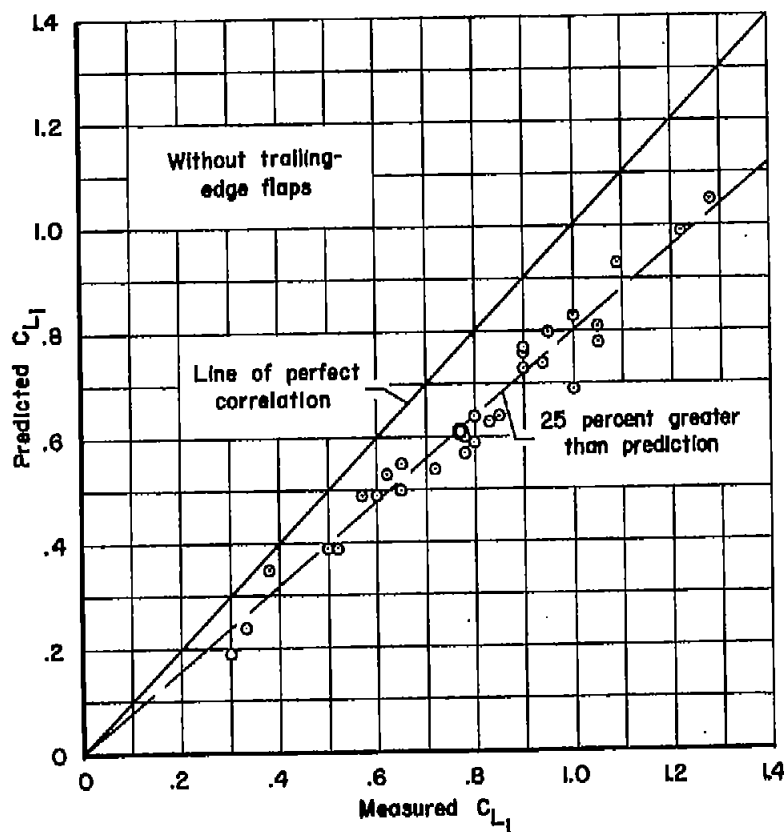
Figure 5.- Correlation of the predicted and measured values of C_{L_1} for several swept-wing plan forms.

	Wing leading edge	① C_{L_f}	② C_{L_a}	③ ①+②	④ 1.15 x ③
——	Plain	.67	.32	.99	1.14
— —	Modified	.67	.55	1.22	1.40
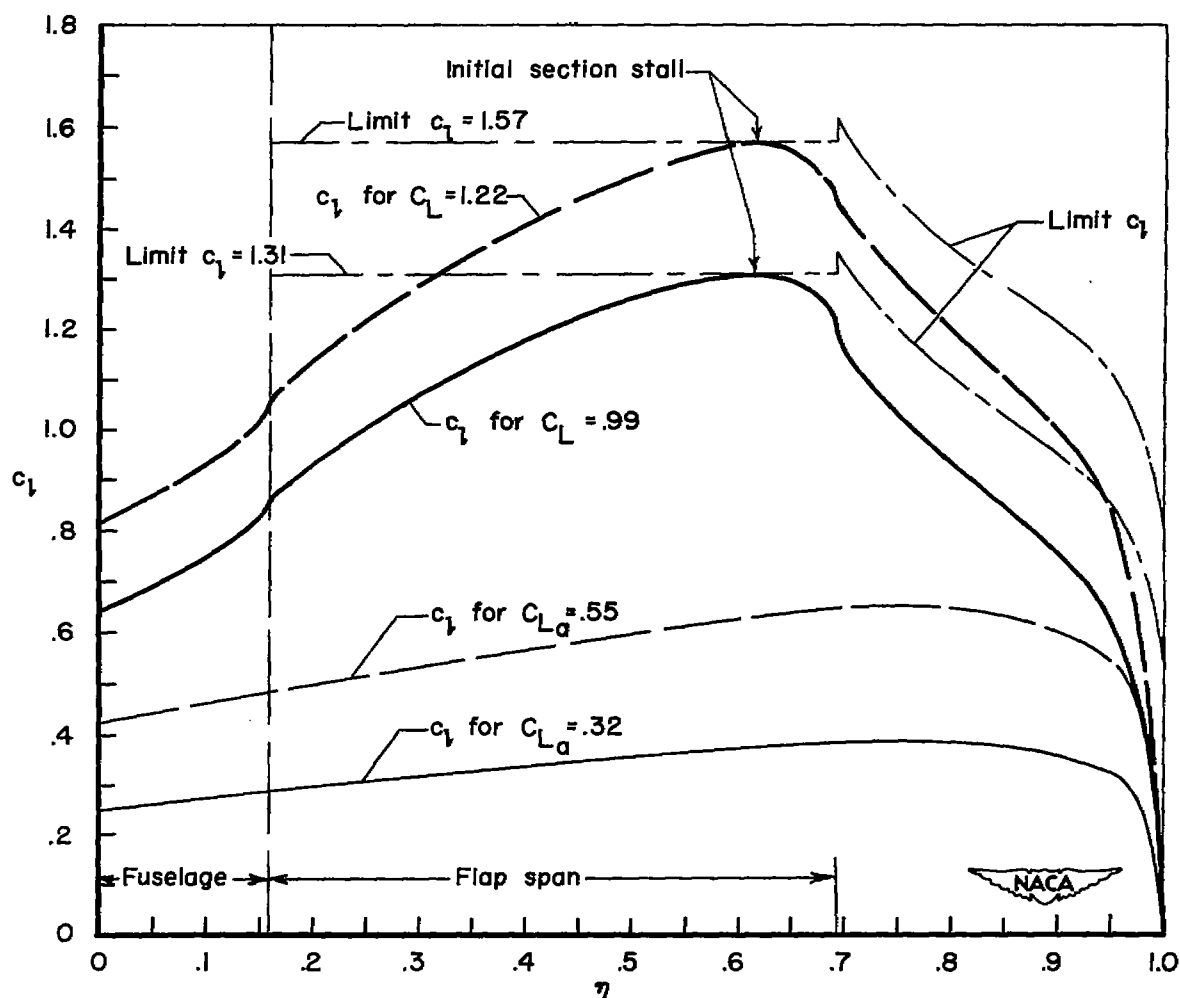
Figure 6.- Theoretical section-lift-coefficient distribution at C_{L_1} for the model with trailing-edge flaps deflected.
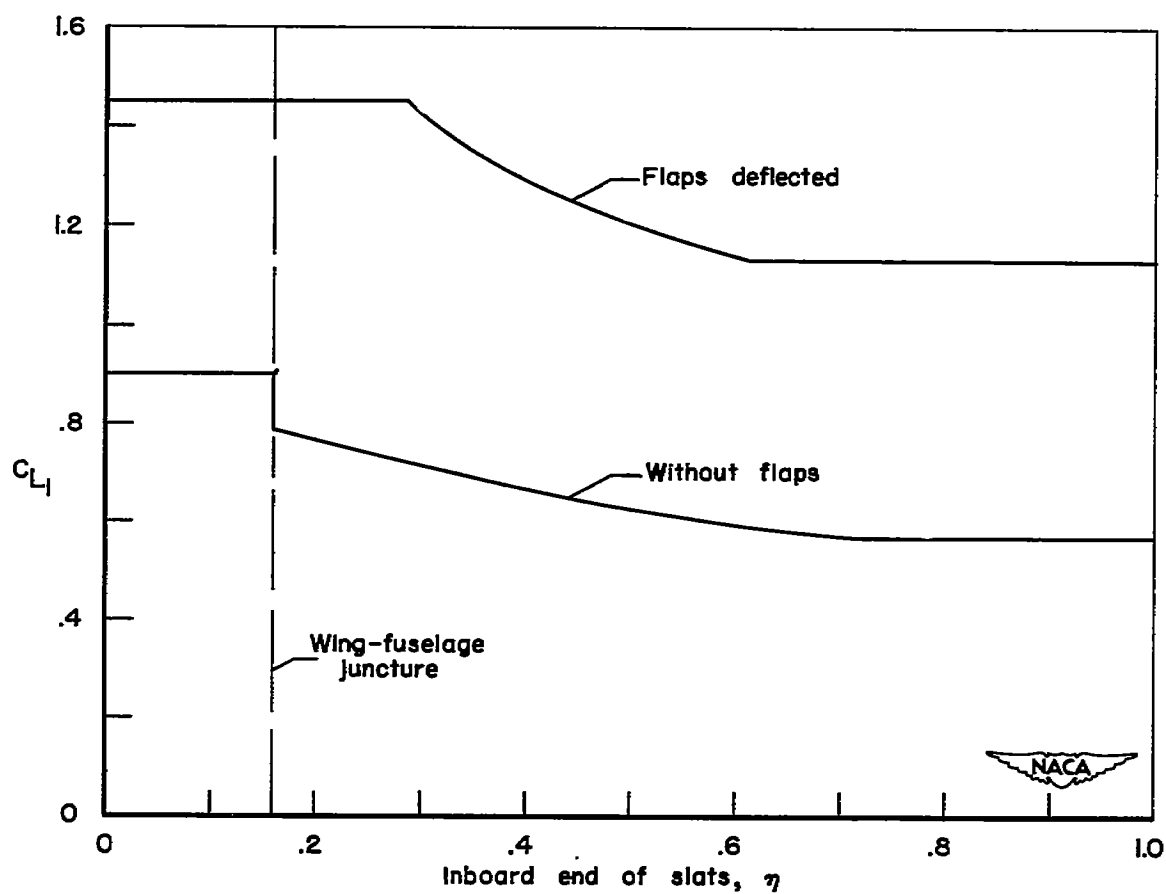
Figure 7.- Variation of C_{L_1} with slat span for the model with and without trailing-edge flaps.
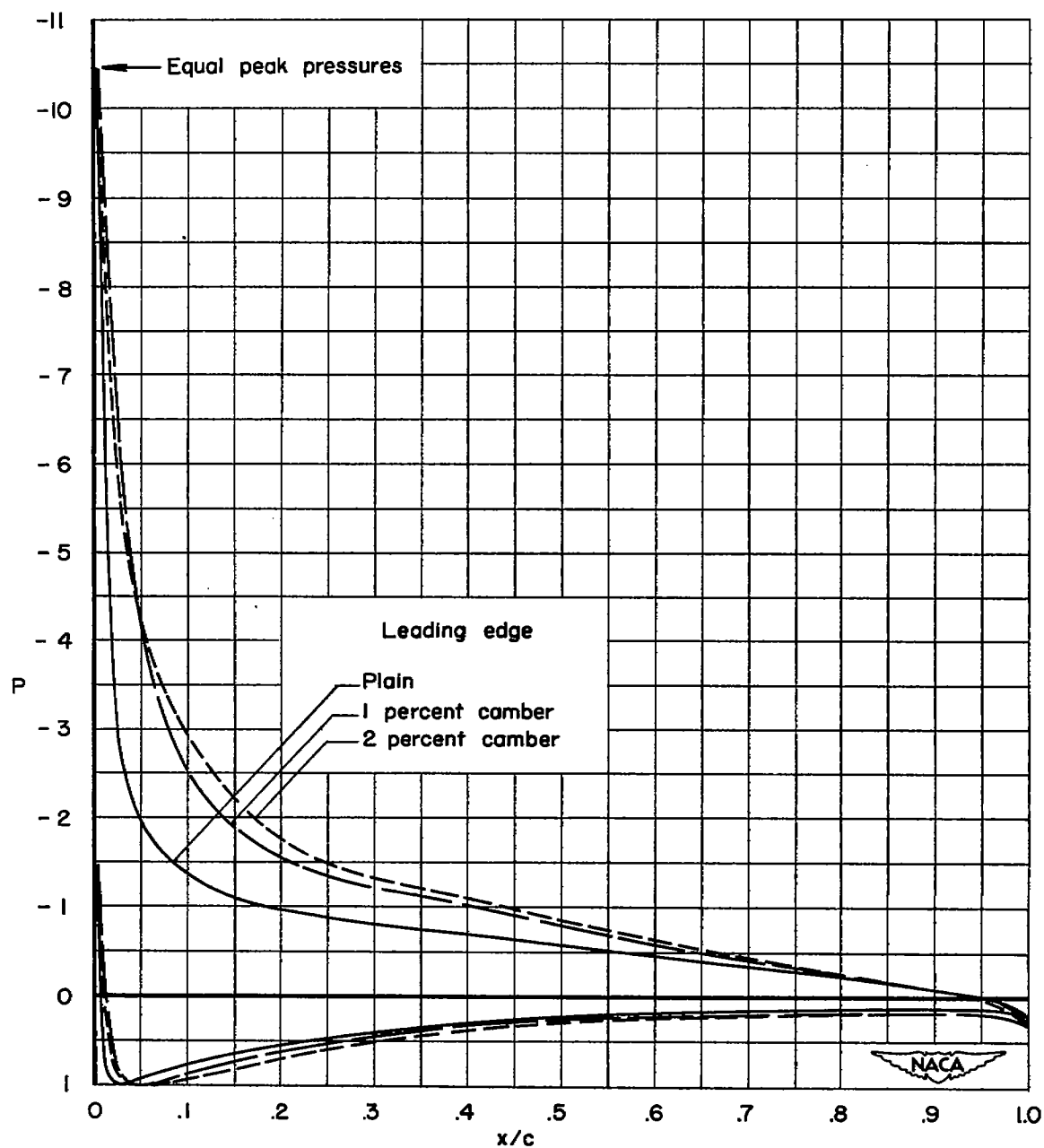
Figure 8.- Theoretical pressure distributions for the NACA 64A010
section with and without modified leading edges at their estimated
$c_{l_{max}}$ values.
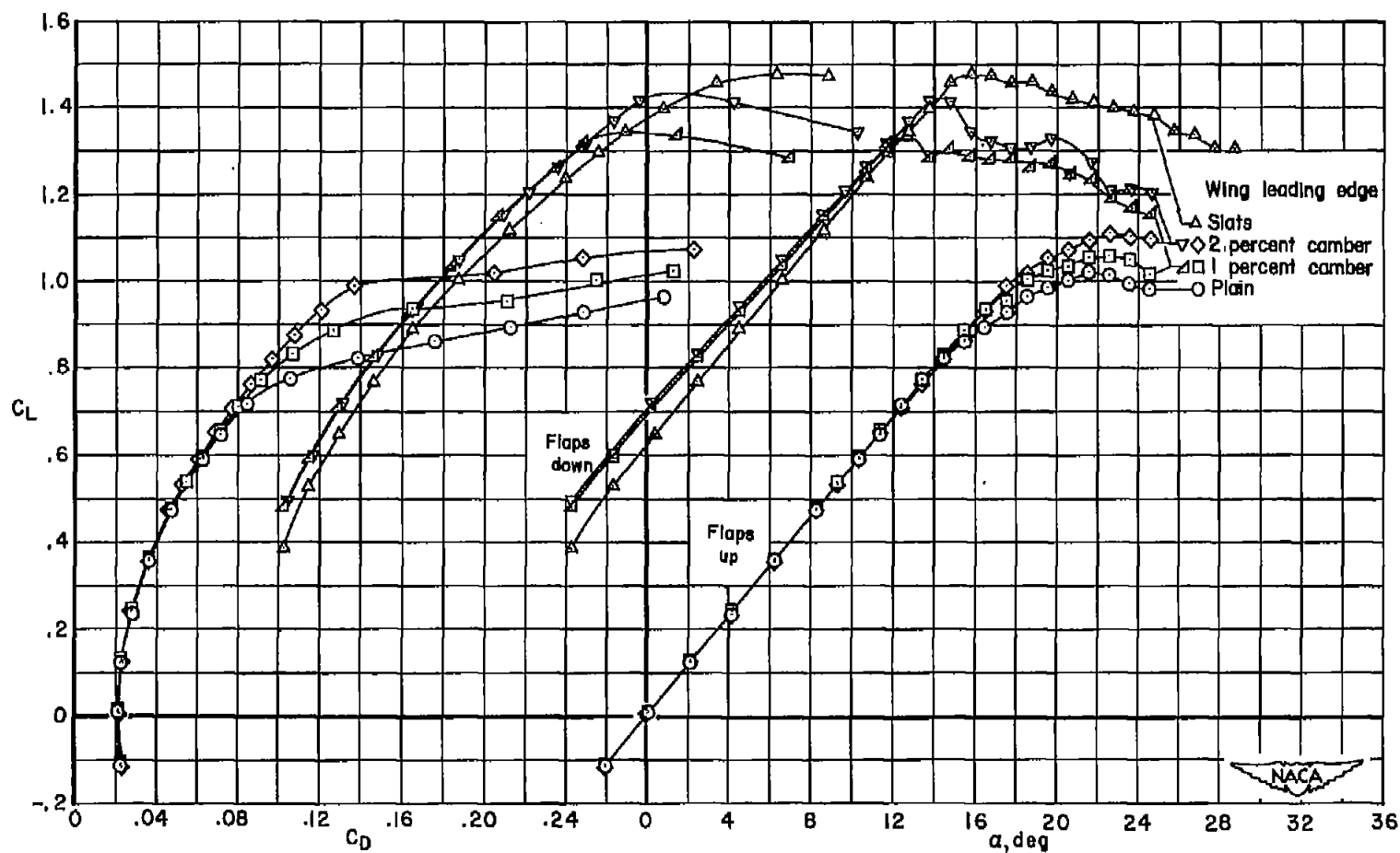
(a) C_D and α vs. C_L

Figure 9.- Aerodynamic characteristics of the wing-fuselage configurations.

Wing leading edge
△ Slats
◇ 2 percent camber ▽
□ 1 percent camber ◁
○ Plain

Flaps down
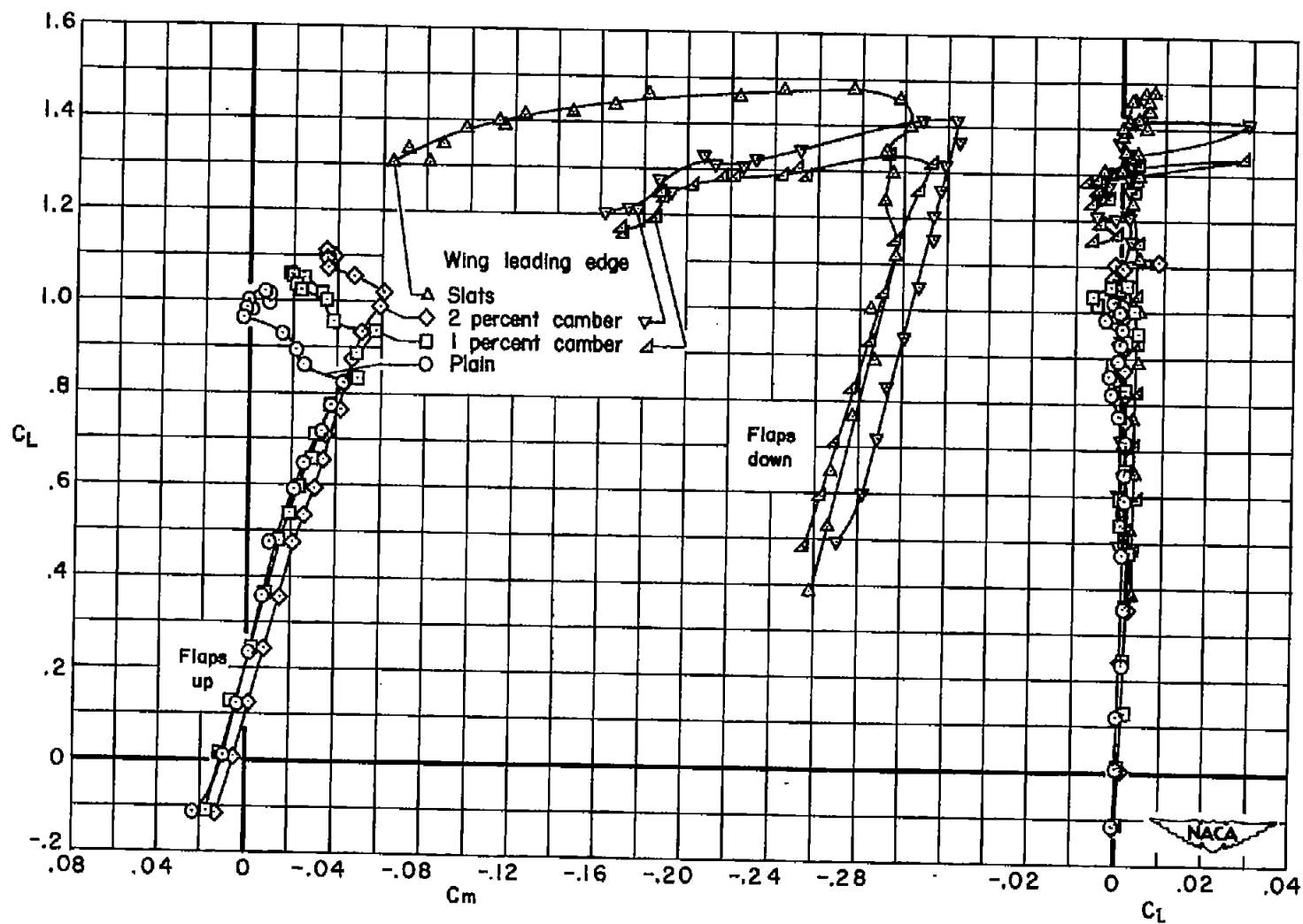
Flaps up

(b) C_l and C_m vs. C_L

Figure 9.- Concluded.
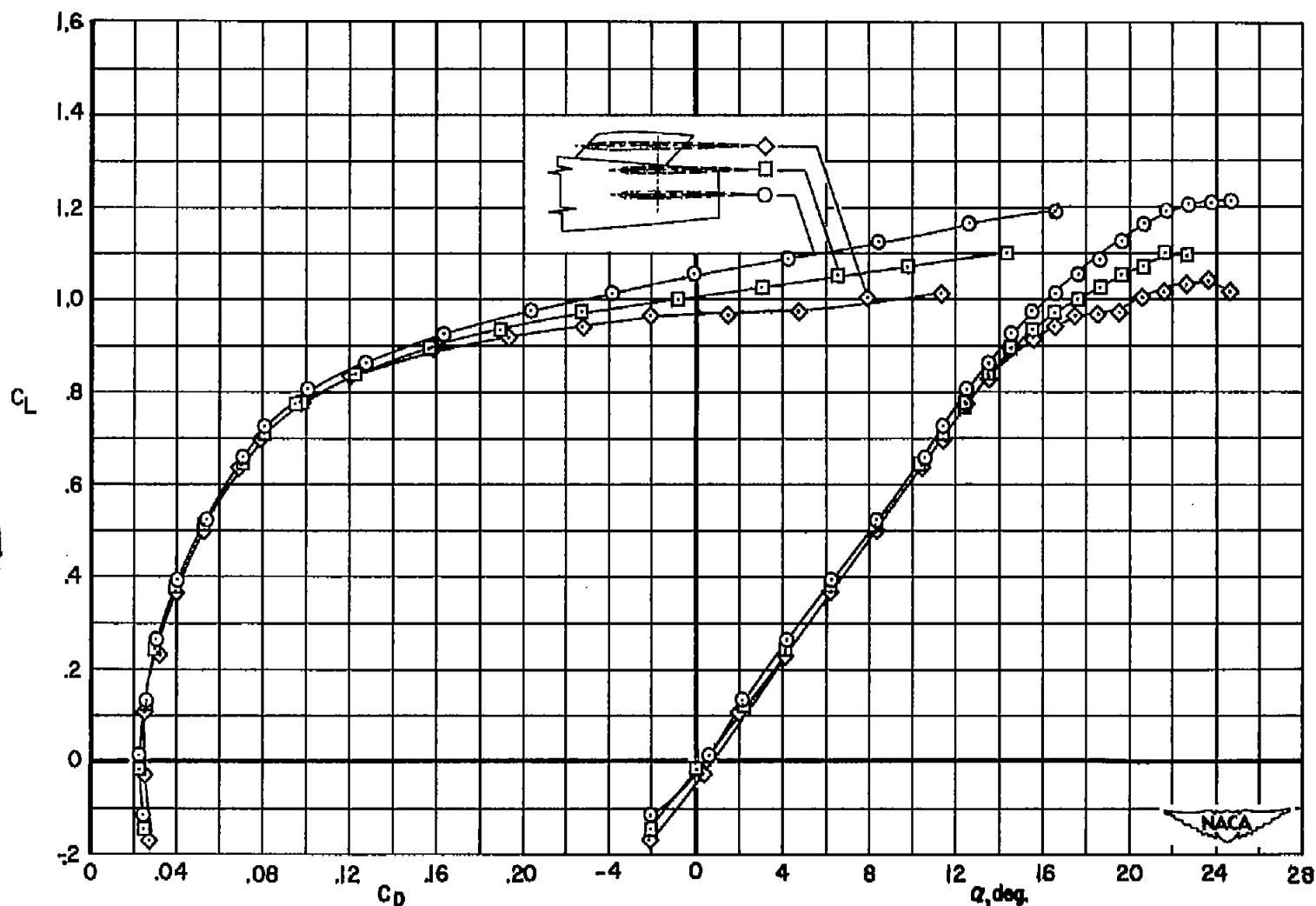
(a) C_D and α vs. C_L

Figure 10.- Aerodynamic characteristics of the complete model with the plain wing leading edge; flaps up; various horizontal tail heights.
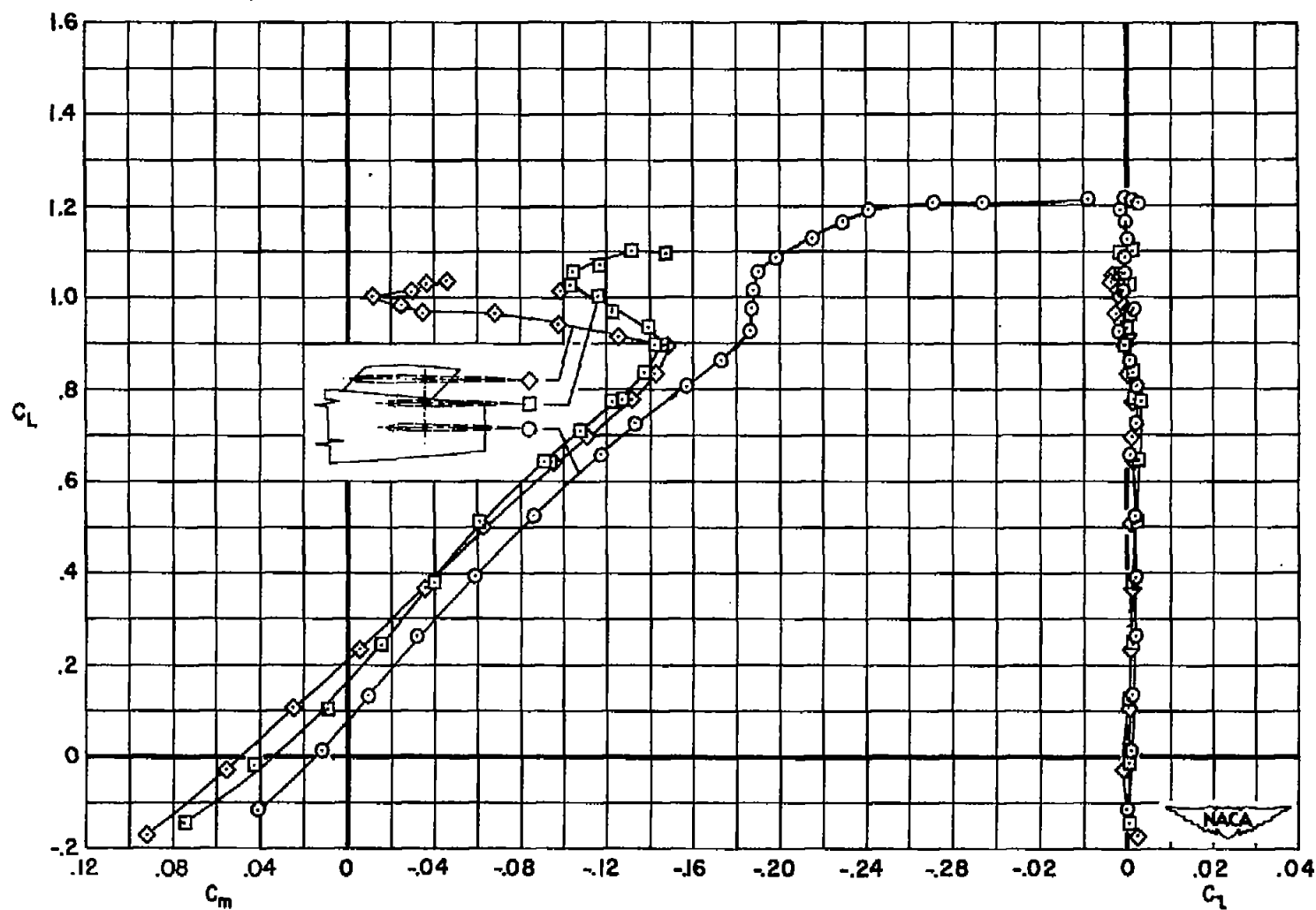
(b) C_l and C_m vs. C_L

Figure 10.- Concluded.
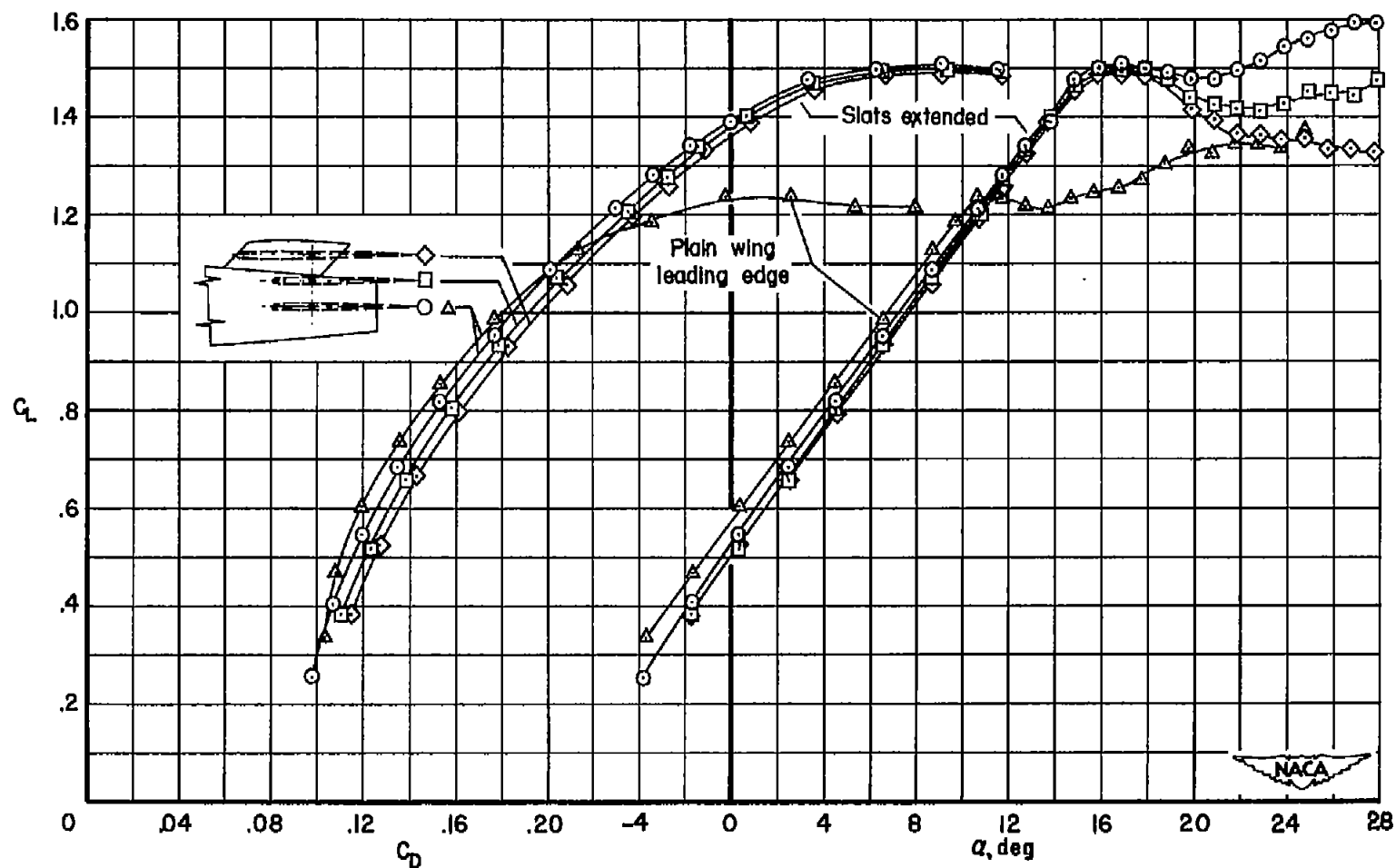
(a) C_D and α vs. C_L

Figure 11.- Aerodynamic characteristics of the complete model with the plain wing leading edge
and with slats extended; flaps down; various horizontal-tail heights.
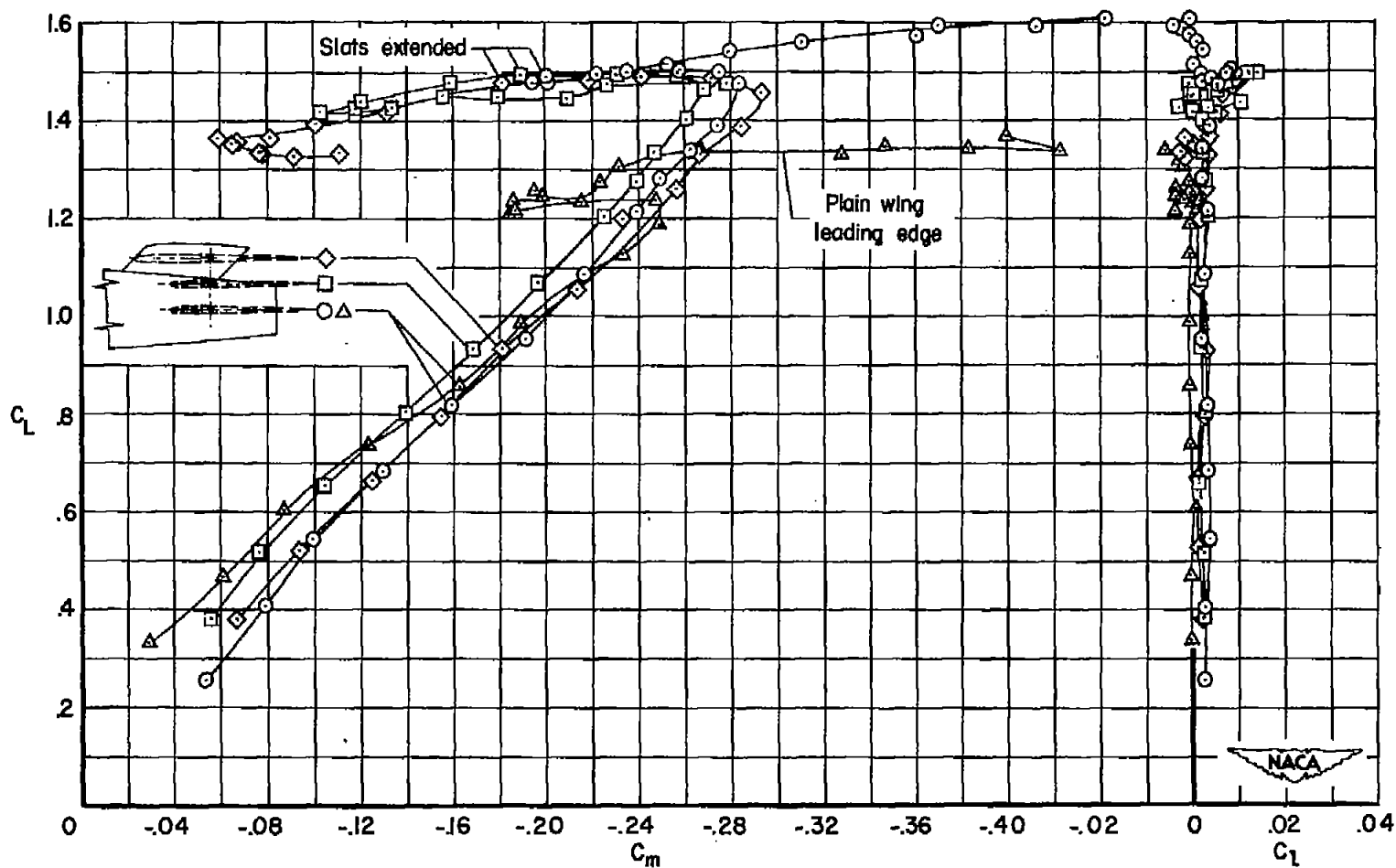
(b) C_l and C_m vs. C_L

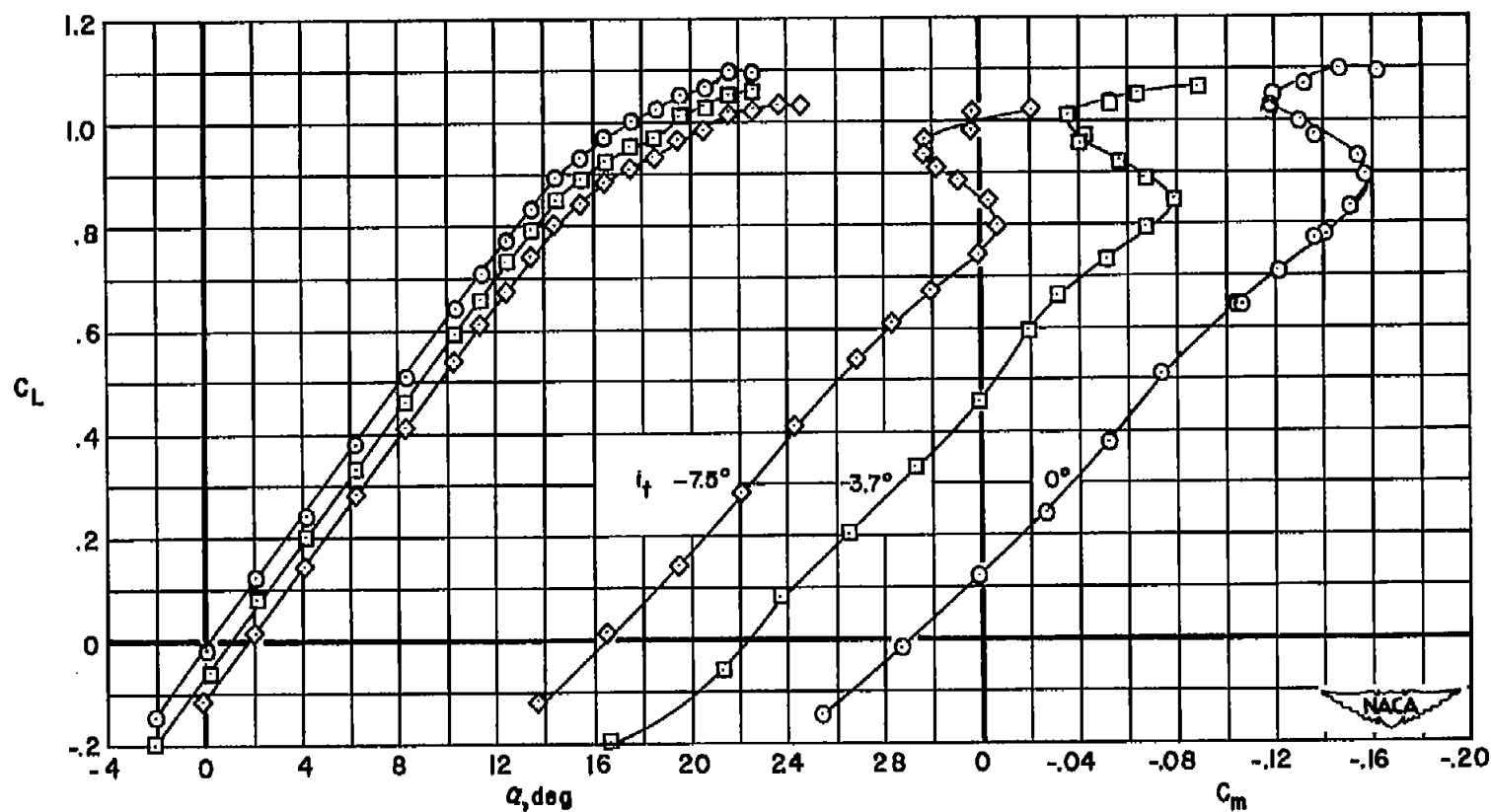Figure 11.- Concluded.
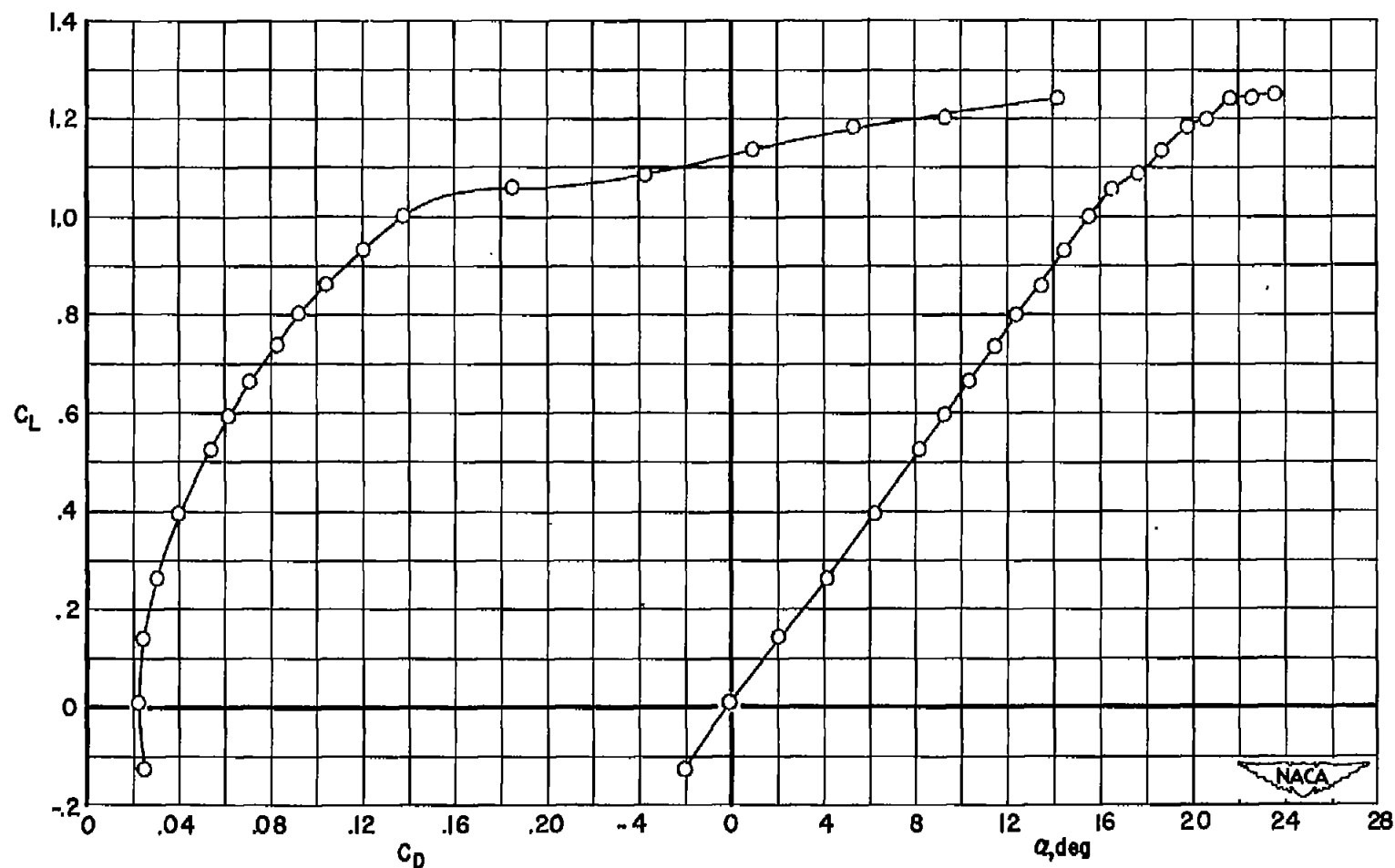
(a) C_D and α vs. C_L

Figure 12.- Aerodynamic characteristics of the complete model with the 1-percent-camber wing leading edge; flaps up; horizontal tail in the low position.

(b) C_l and C_m vs. C_L

Figure 12.- Concluded.
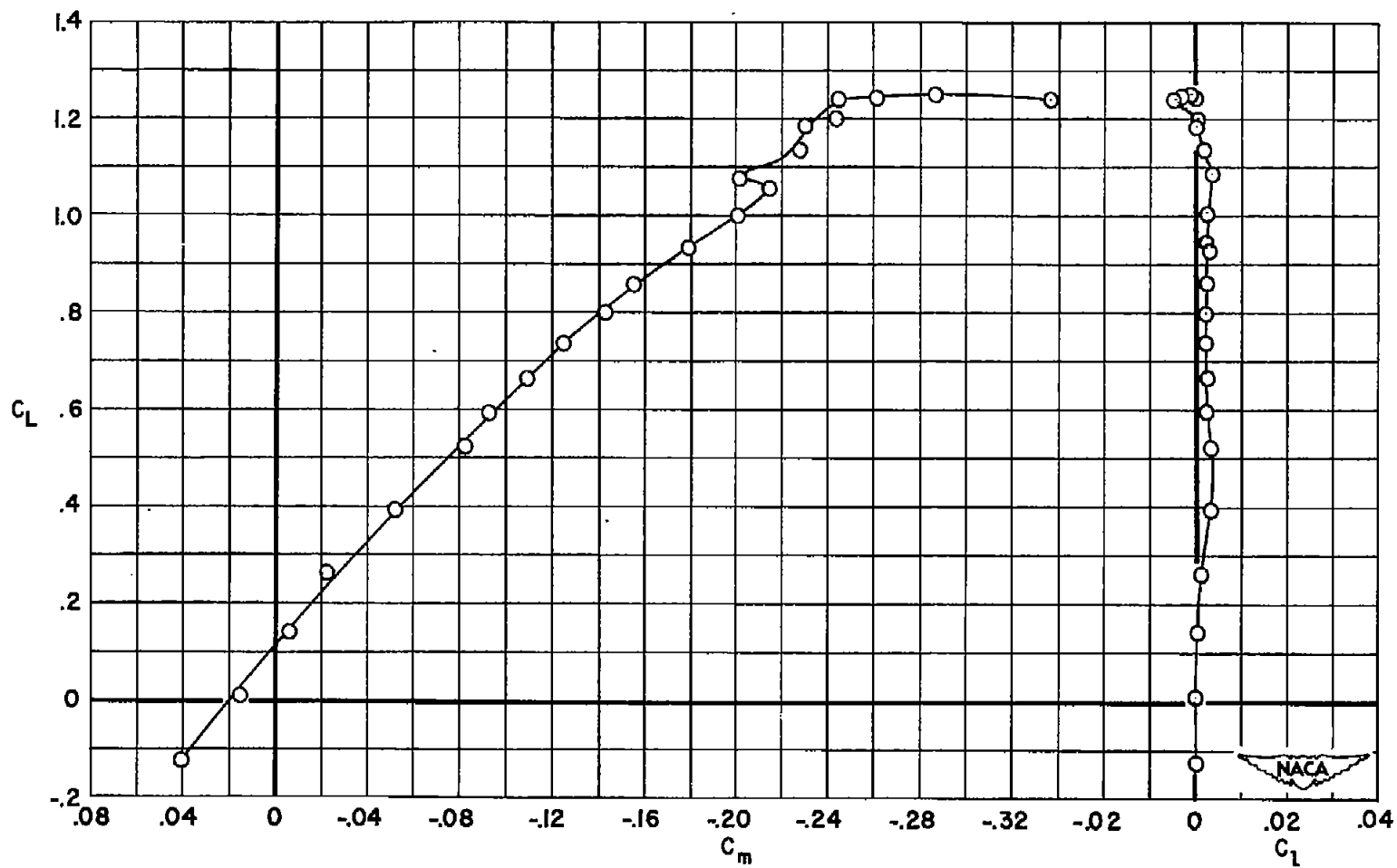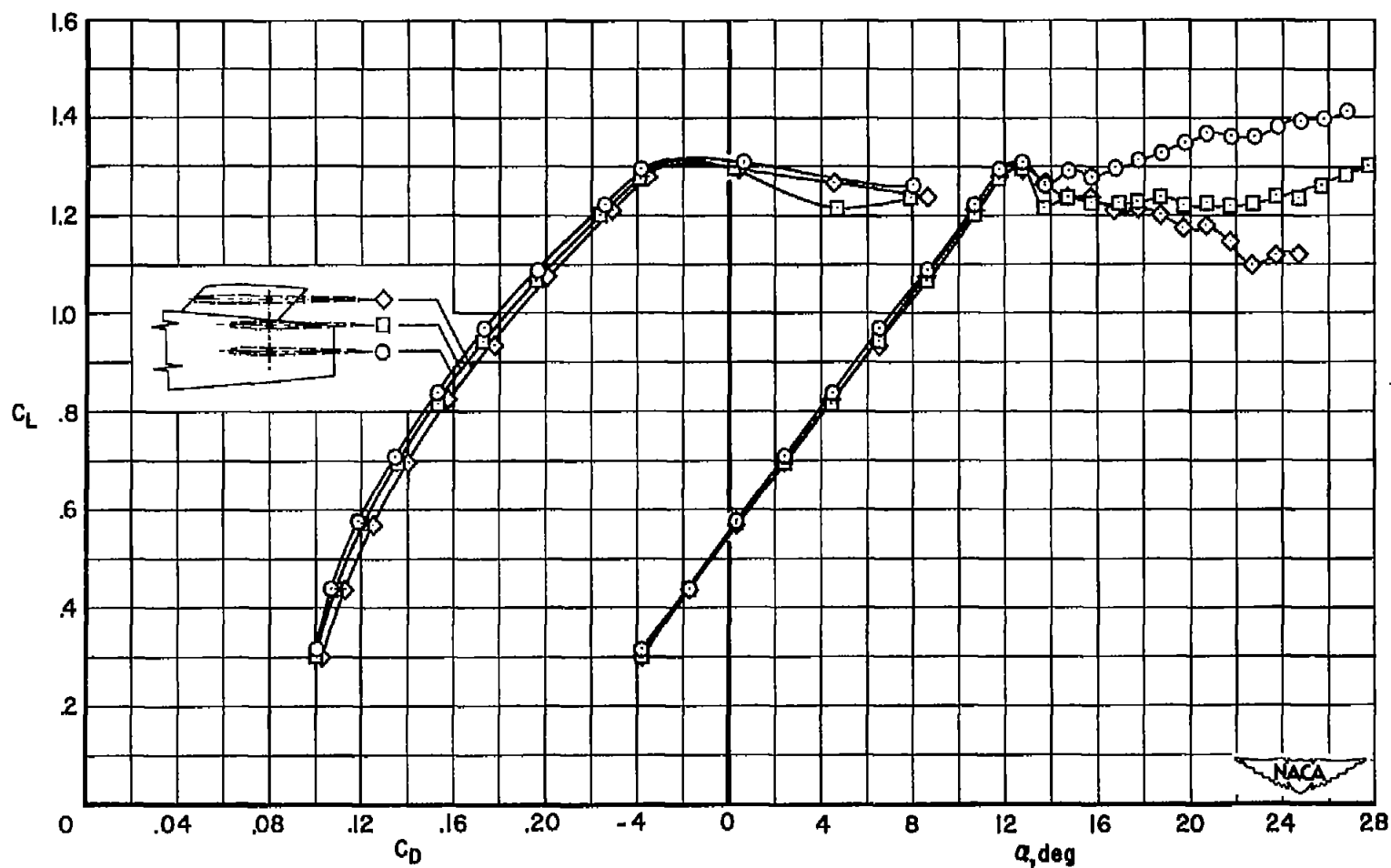
(a) C_D and α vs. C_L

Figure 13.- Aerodynamic characteristics of the complete model with the 1-percent-camber wing leading edge; flaps down; various horizontal-tail heights.
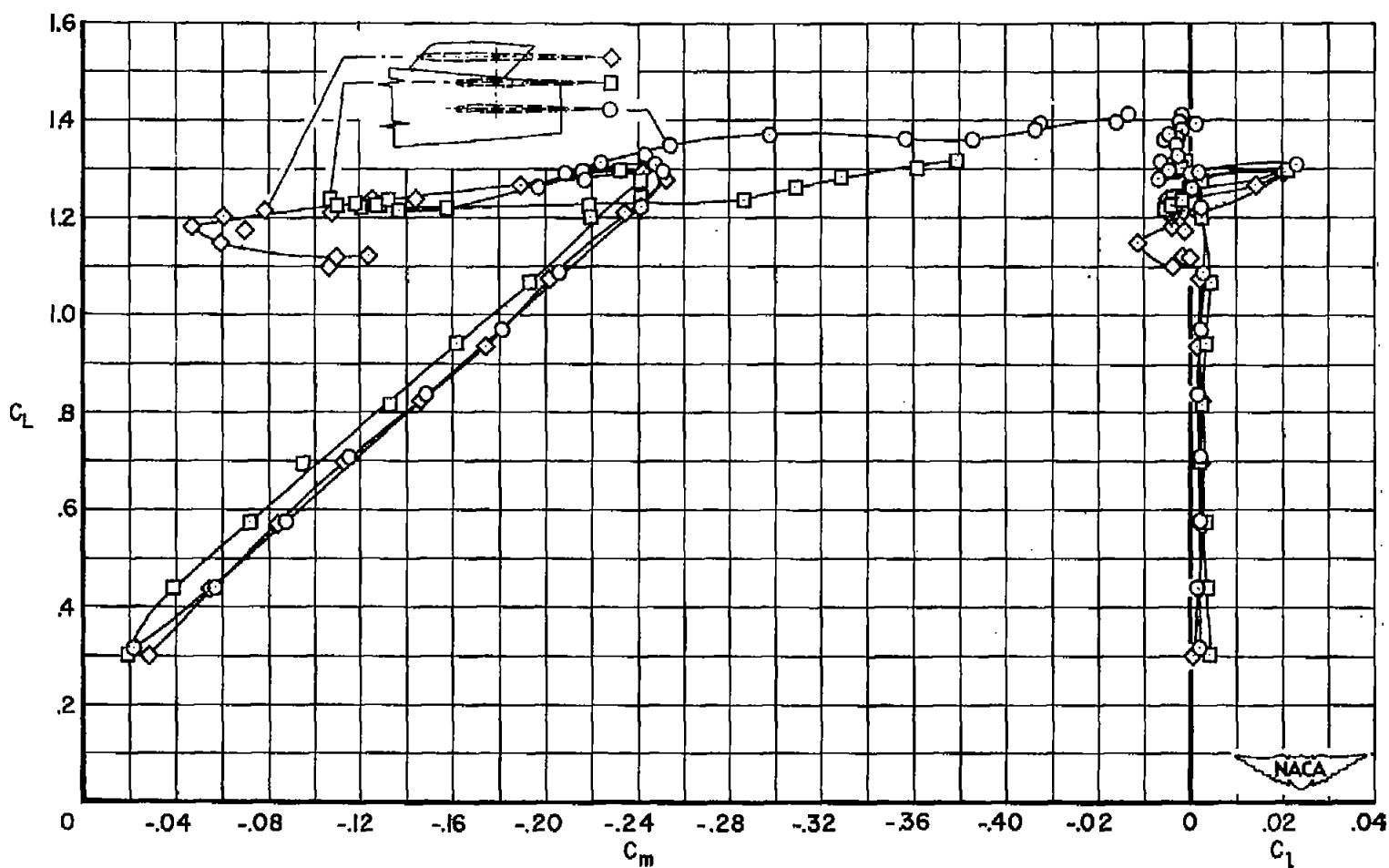
(b) C_l and C_m vs. C_L

Figure 13.- Concluded.
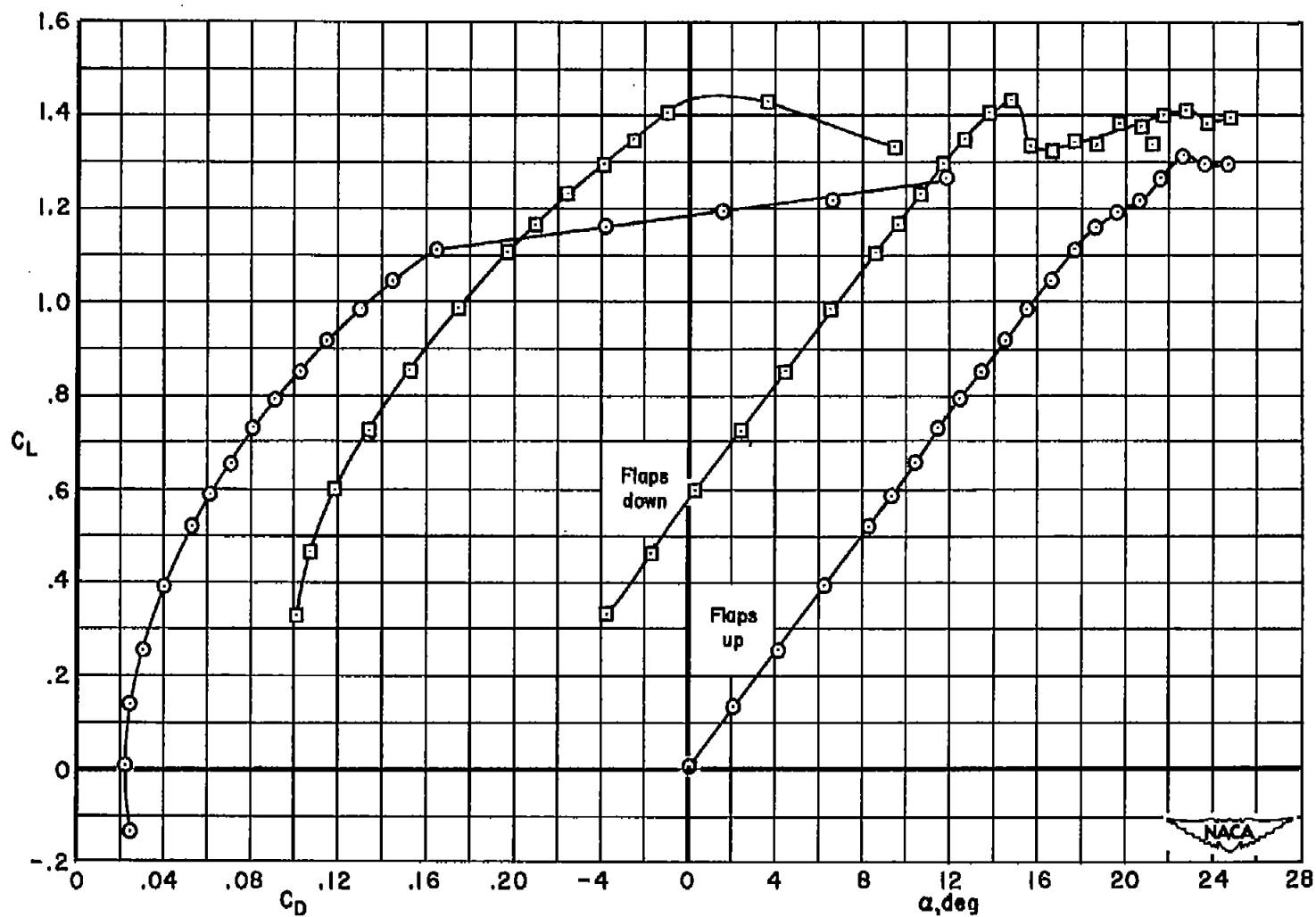
(a) C_D and α vs. C_L

Figure 14.- Aerodynamic characteristics of the model with the 2-percent-camber wing leading edge; horizontal tail in the low position.
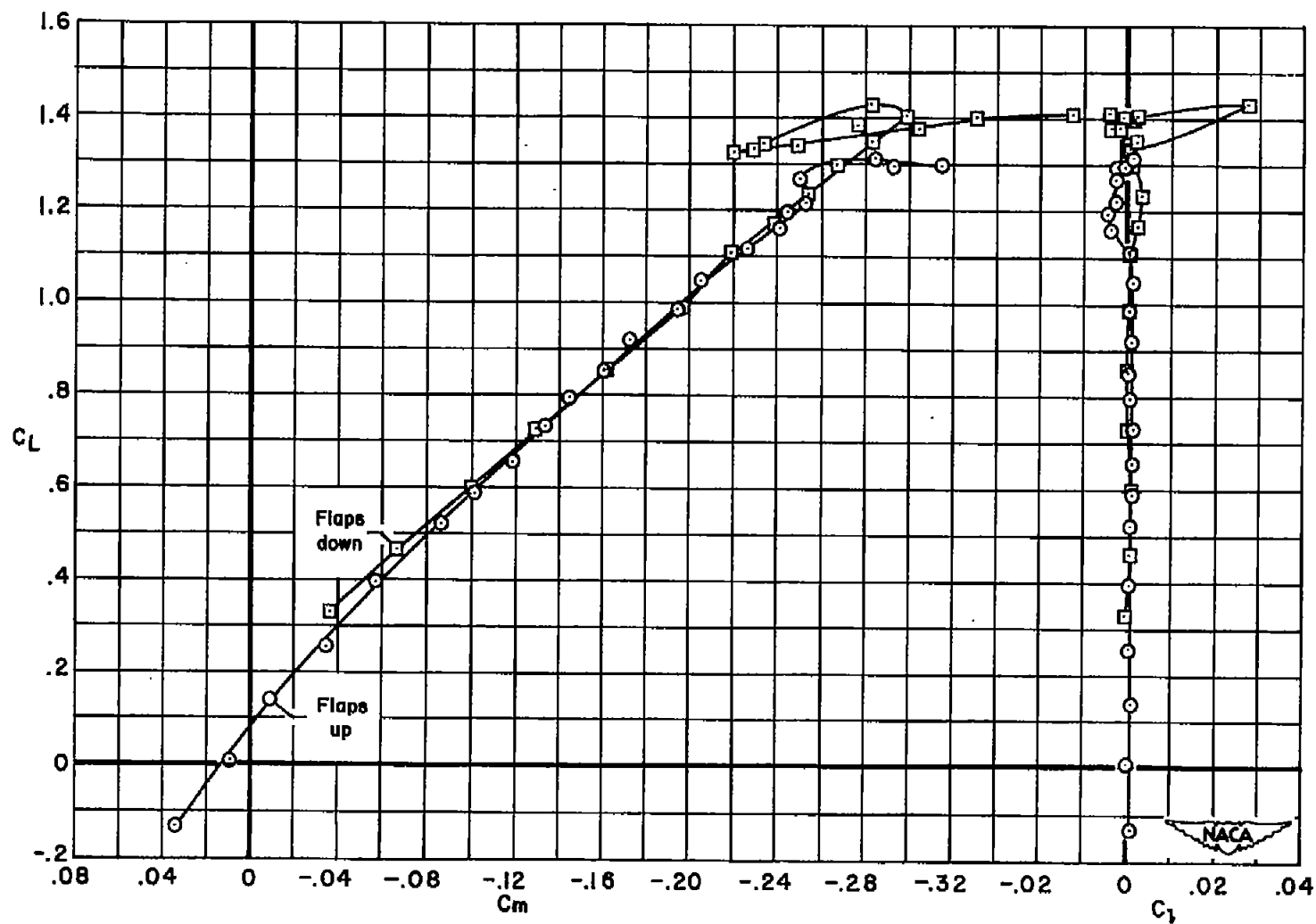
(b) C_l and C_m vs. C_L

Figure 14.- Concluded.
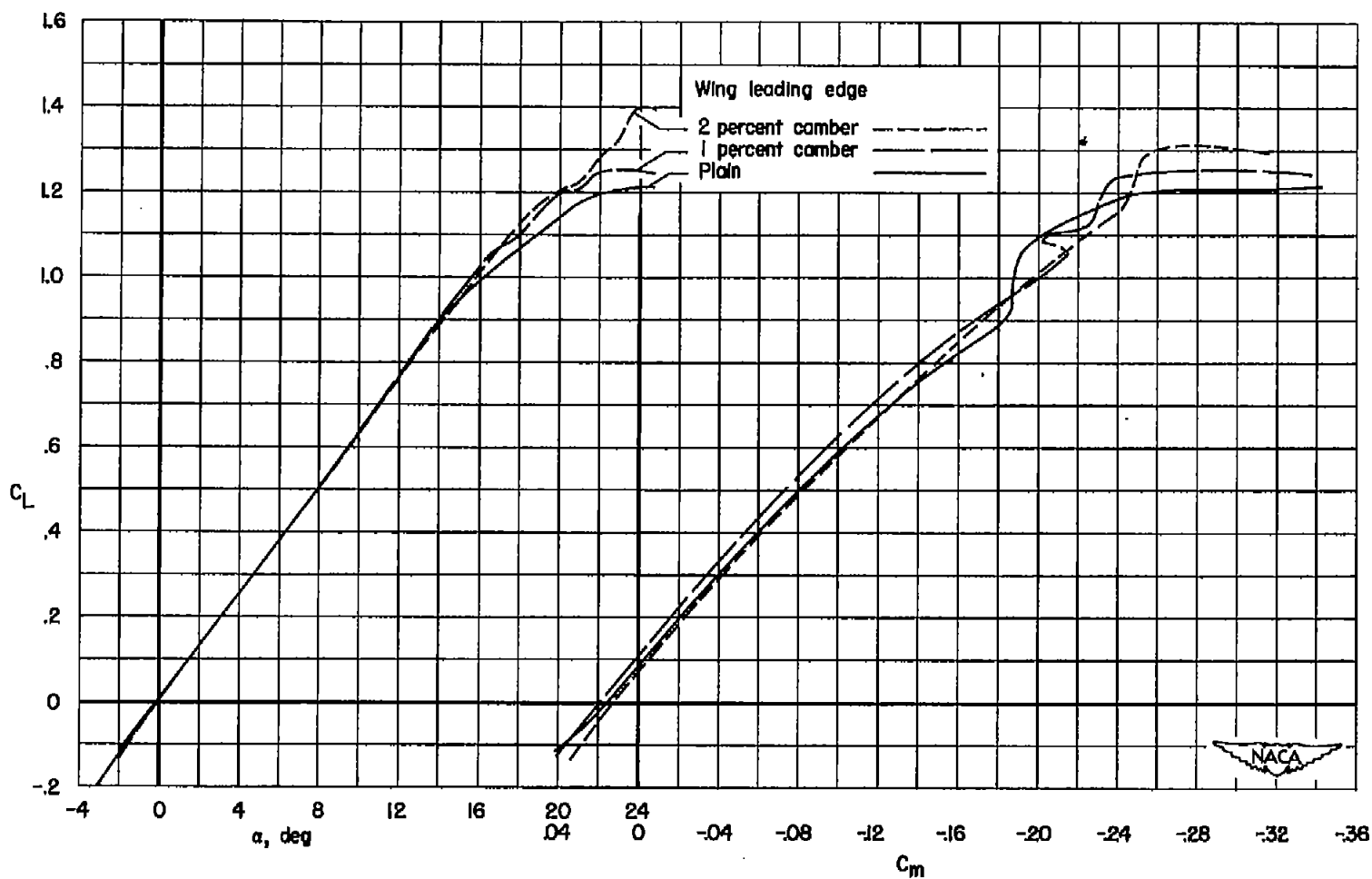
(a) Flaps up.

Figure 15.- Lift and pitching-moment characteristics of the model with the horizontal tail in the low position.
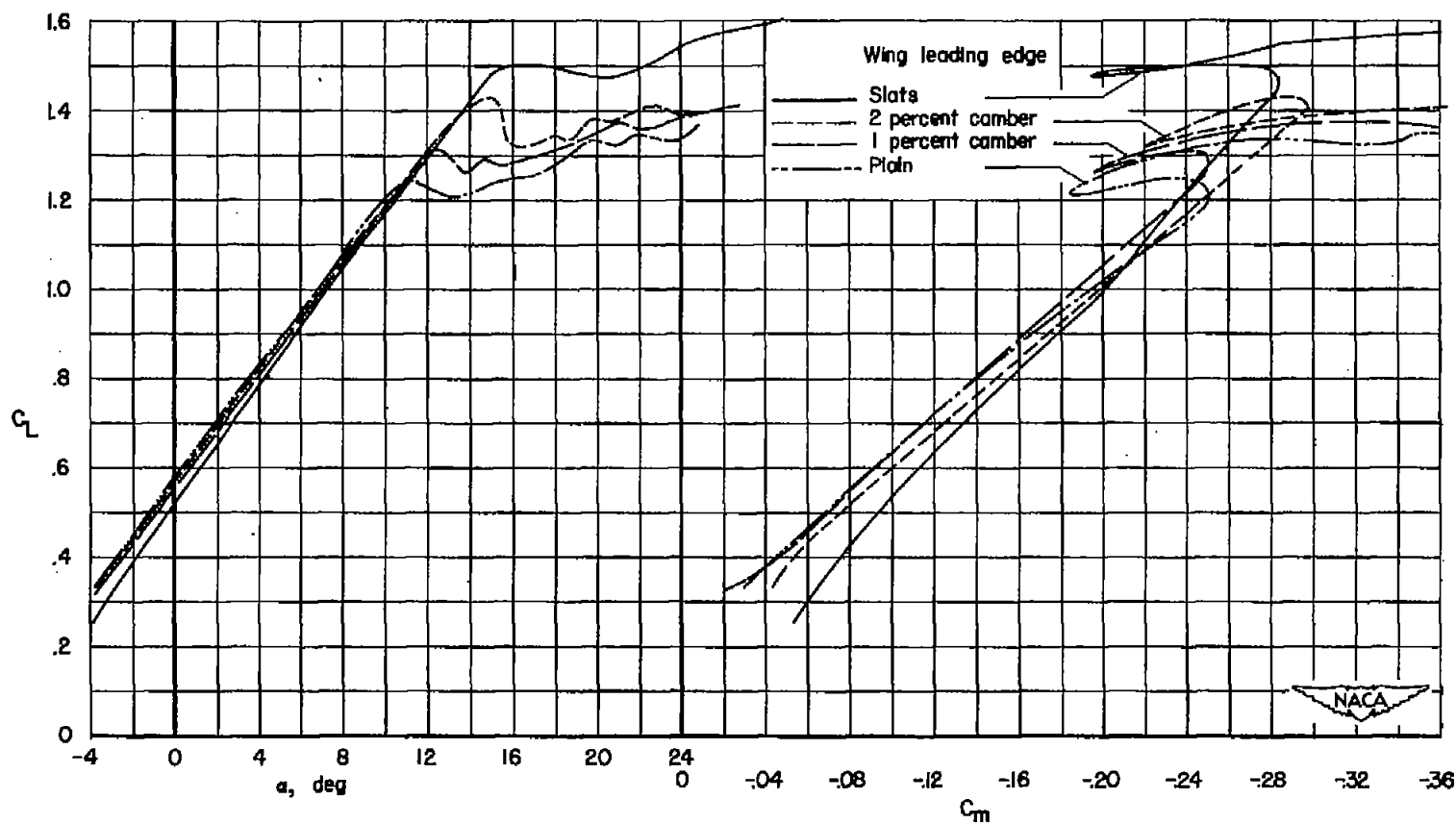
(b) Flaps deflected.
Figure 15.- Concluded.

Figure 16.- Aerodynamic characteristics of the complete model with the plain wing leading edge; flaps up; horizontal tail in the mid-position; various tail incidences.
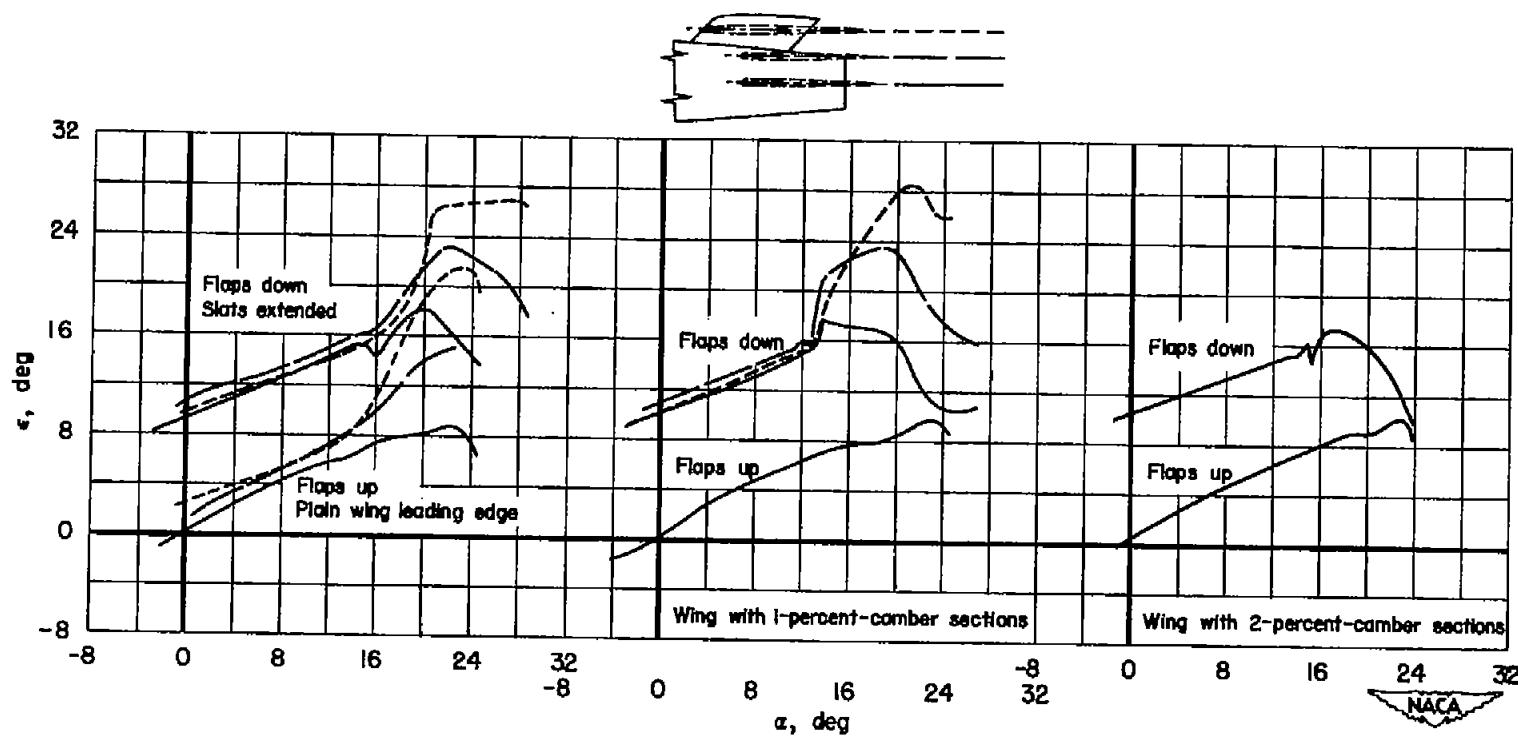
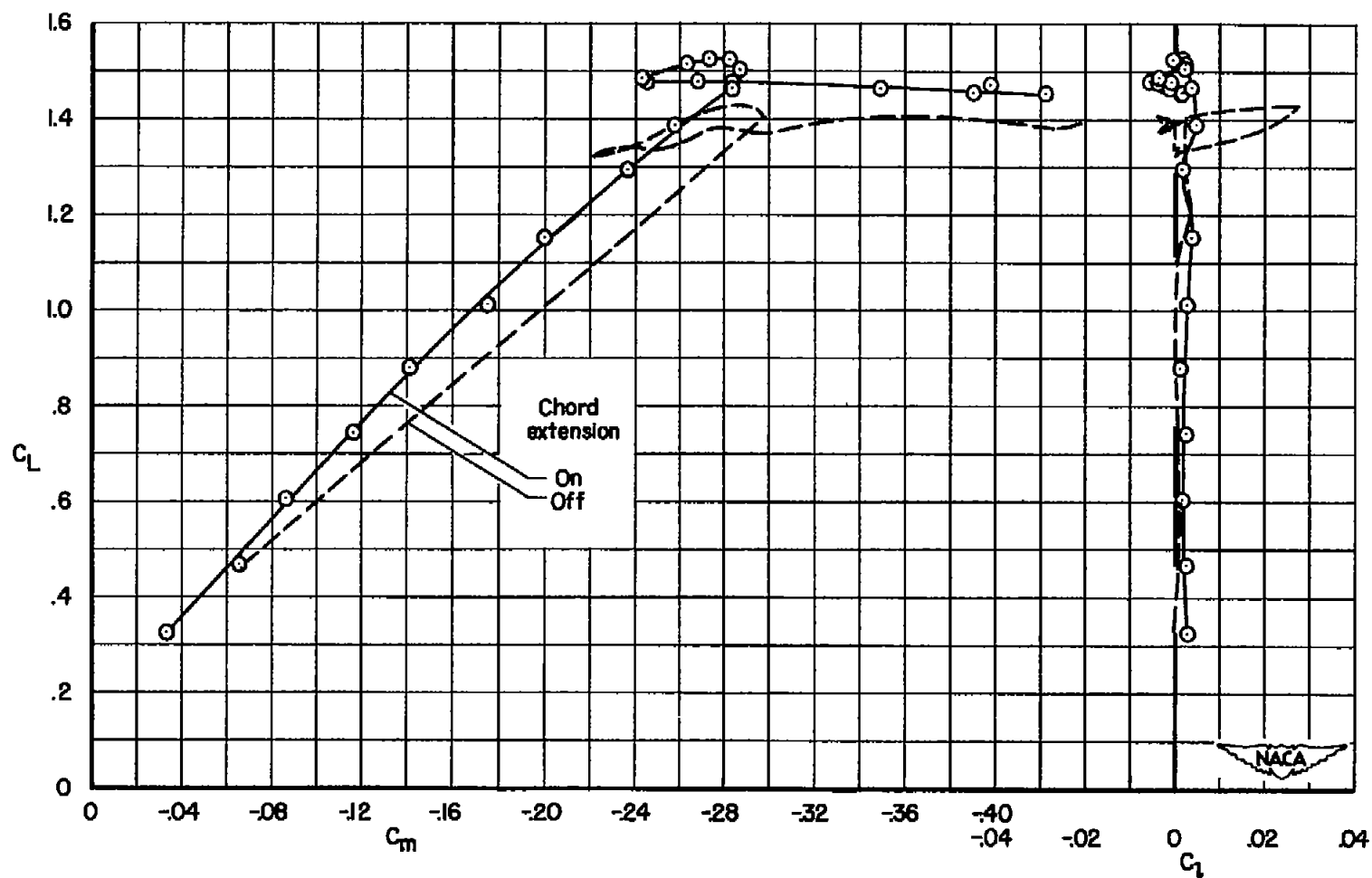Figure 17.- Downwash characteristics at the horizontal tail.
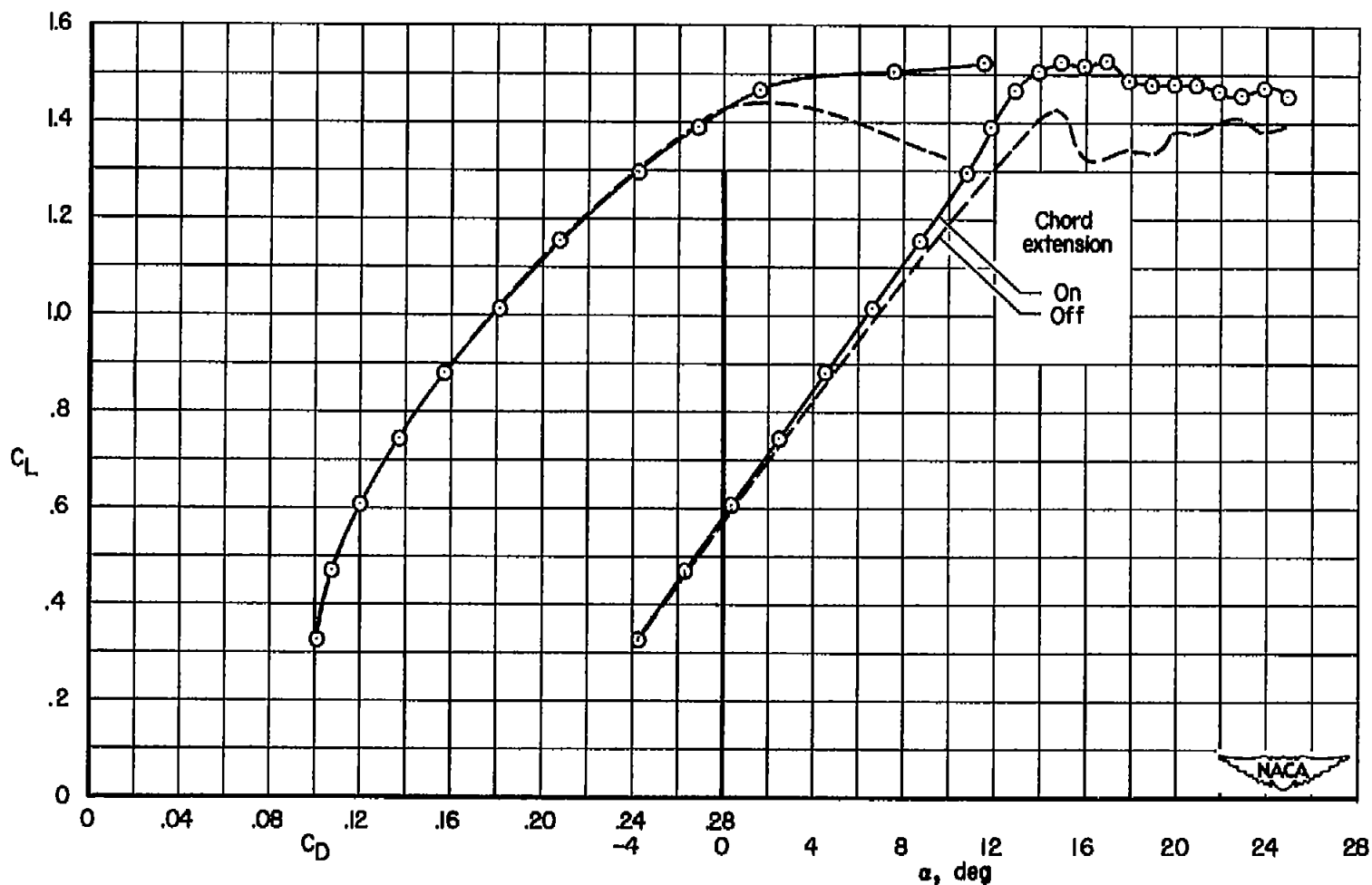
(a) C_D and α vs. C_L

Figure 18.- Effects of a half-span, wing, leading-edge, chord extension on the aerodynamic char-
acteristics of the model with 2-percent-camber sections; flaps down; low horizontal tail.
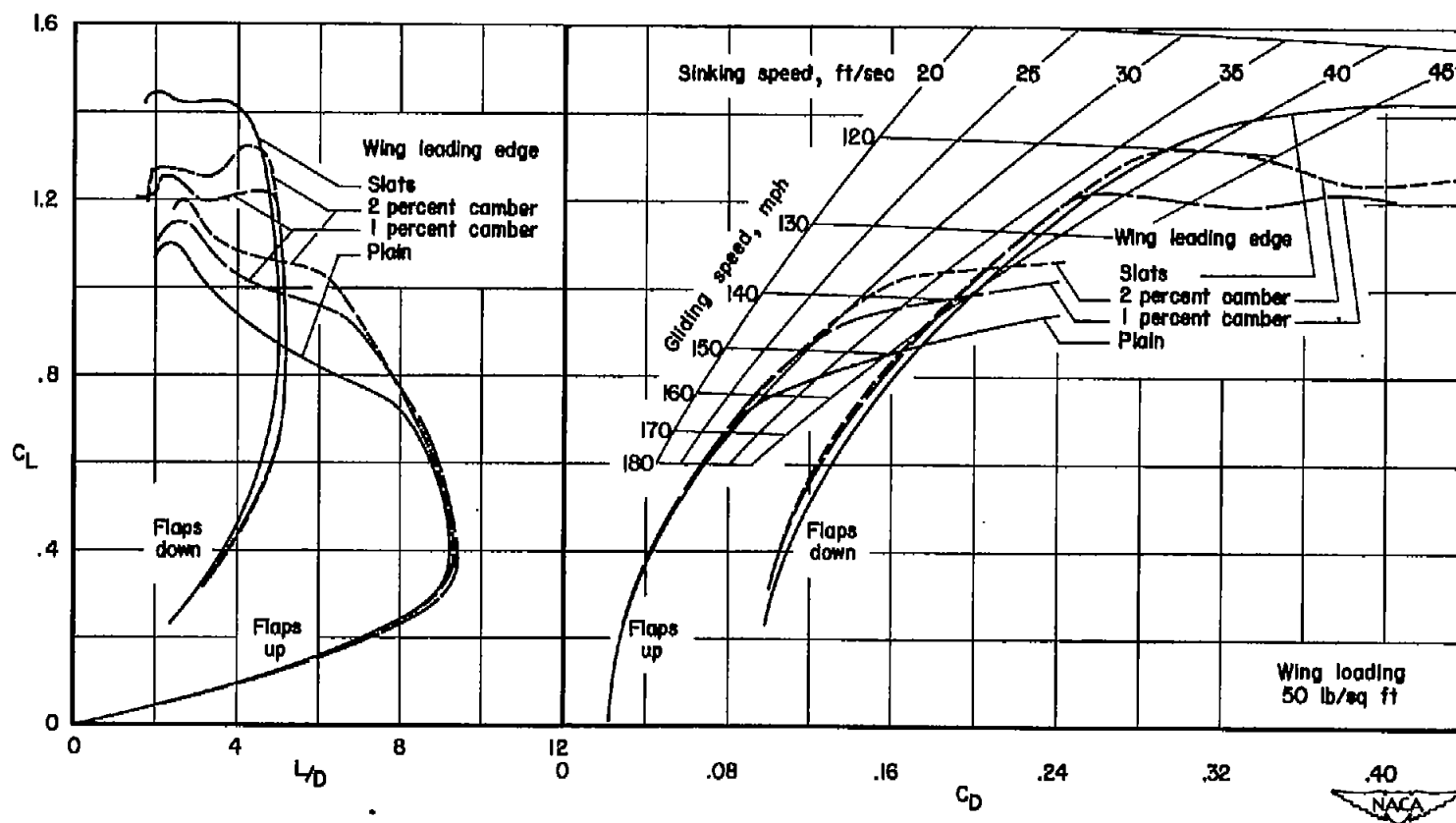
(b) C_l and C_m vs. C_L

Figure 18.- Concluded.

Figure 19.- The lift-drag ratios and power-off-glide sink-speed characteristics of the models with the tail in the low position trimmed with a center of gravity located at 0.31c̄.
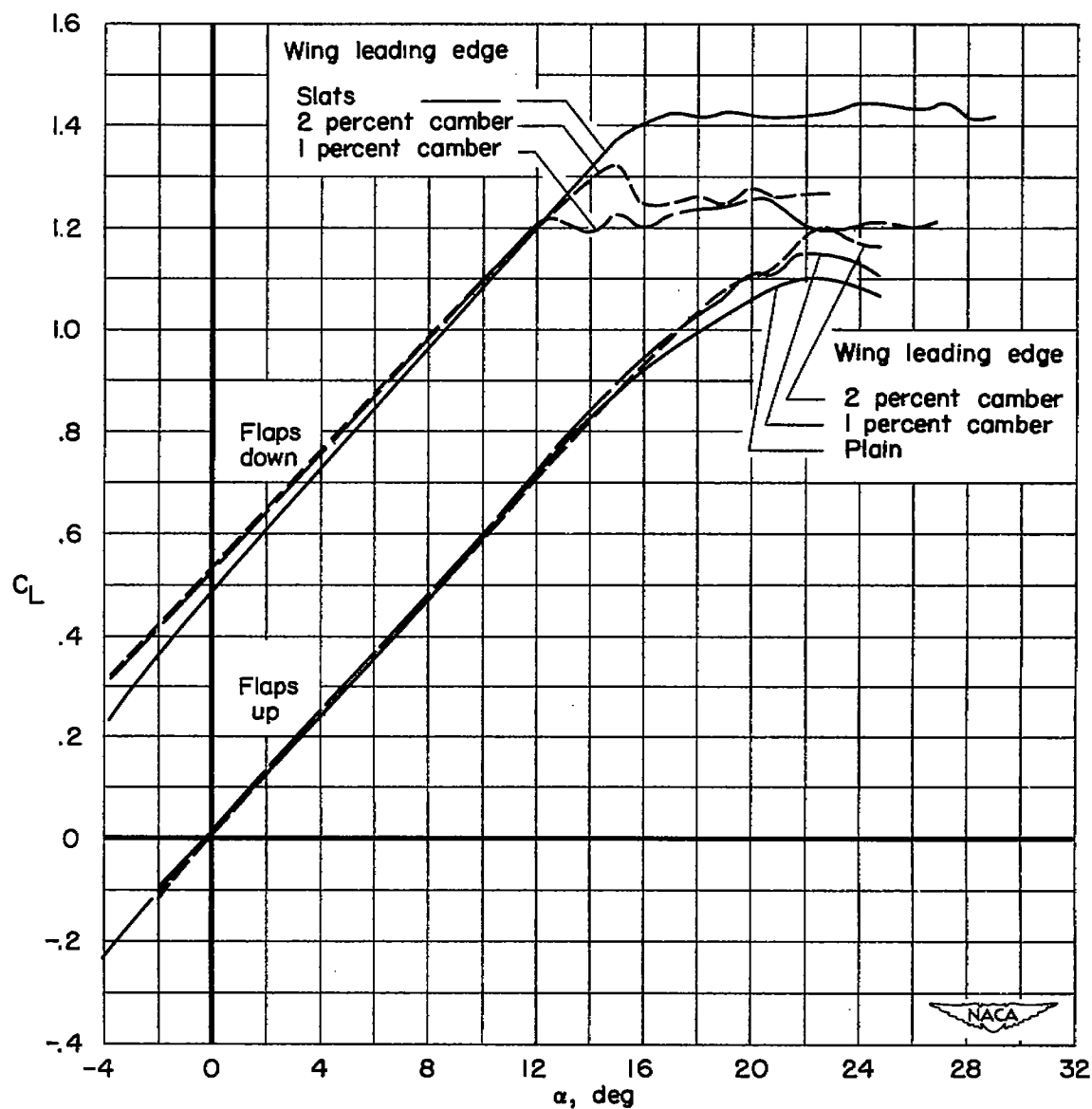
Figure 20.- Lift characteristics of the models with the horizontal tail in the low position trimmed with a center of gravity located at $0.31\bar{c}$.